Supplementary Information

p53 destabilizing protein skews asymmetric division and enhances NOTCH activation to direct self-renewal of TICs

Authors: Hye Yeon Choi, Hifzur R. Siddique, Mengmei Zheng, Yi Kou, Da-Wei Yeh, Tatsuya Machida, Chia-Lin Chen, Dinesh Babu Uthaya Kumar, Vasu Punj, Peleg Winer, Alejandro Pita, Linda Sher, Stanley M. Tahara, Ratna B. Ray, Chengyu Liang, Lin Chen, Hidekazu Tsukamoto, Keigo Machida*

*Correspondence to: keigo.machida@med.usc.edu

This PDF file includes:

Supplementary Table 1. Box plot statistics

	Normal	Early stage	Late Stage
Upper whisker	9.76	12.57	17.08
3rd quartile	6.73	11.27	15.34
Median	5.36	9.71	14.71
1st quartile	3.93	7.05	14.03
Lower whisker	2.95	0.98	12.83
Number of samples	62	284	102
Average expression	5.57	8.82	14.72
minimum expression	3	0.1	13
Maximum expression	10	12	18

Methodology:

From public datasets (TCGA, GSE17856) of liver cancer patients showing gene expression and matched clinical data, a subset of data showing gene expression corresponding to various stages of liver cancer including metastasis was generated. The samples were divided into early stage and late metastatic stage of tumor progression to correlate the expression of Notch1 and TBC1D15 in tumor progression. The early stage non-metastatic samples showed an average combined expression of both genes as 8.8 (range of 0.1-12), while late stage metastatic samples with an average of 14.7 (range 13- 18). A t-test was performed to estimate the differences in the expression of Notch1 and TBC1D15 genes in early and late metastatic stage of liver cancer patients as well as normal non tumor individuals.

- **Supplementary Table 2**

REAGENT OR RESOURCE	SOURCE	IDENTIFIER
Antibodies		
Anti-Notch1 antibody – ChIP Grade	Abcam	ab27526
Anti-Notch1 antibody [EP1238Y]	Abcam	ab52627
Anti-Notch1 antibody [A6]	Abcam	ab44986
Anti-Nanog antibody – ChIP Grade	Abcam	ab21624
Anti-Aurora A antibody [35C1]	Abcam	ab13824
Anti-GFP antibody [9F9.F9]	Abcam	ab1218
NOTCH2 antibody [C2], C-term	GeneTex	GTX101593
TBC1D15 antibody [N1N2], N-term	GeneTex	GTX121082
HA tag antibody [GT423]	GeneTex	GTX628489
RANGAP1 antibody [1B4]	GeneTex	GTX83725
NuMA antibody [GT3611]	GeneTex	GTX629397
Anti-Aurora-A Kinase antibody, Mouse monoclonal	Sigma Aldrich	A1231
Anti-TBC1D15 antibody produced in rabbit	Sigma Aldrich	HPA013388
Anti-c-Myc Tag antibody produced in rabbit	Sigma Aldrich	SAB4301136
Monoclonal Anti-HA antibody produced in mouse	Sigma Aldrich	H9658
HA Tag Monoclonal Antibody (2-2.2.14)	Thermo Fisher Scientific	26183
TBC1D15 Antibody	NOVUS BIOLOGICALS	NBP1-90503
Anti-Myc Tag Antibody, clone 4A6	EMD Millipore Corp	05-274
p53 (1C12) Mouse mAb	Cell Signaling Technology	2524
Phospho-Numb (Ser276) Antibody	Cell Signaling Technology	4140
Nanog (D1G10) Rabbit mAb (Mouse Specific; ChIP Formulated)	Cell Signaling Technology	8785
Notch1 (D6F11) XP Rabbit mAb	Cell Signaling Technology	4380
N1ICD (Val 1744) (D3B8) Rabbit mAb	Cell Signaling Technology	4147
Numb (C29G11) Rabbit mAB	Cell Signaling Technology	**2756**
Notch1 (D1E11) XP Rabbit mAb	Cell Signaling Technology	3608
Notch2 (D76A6) XP Rabbit mAb	Cell Signaling Technology	5732
Notch3 (D11B8) Rabbit mAb	Cell Signaling Technology	5276
Notch4 (L5C5) Mouse mAb	Cell Signaling Technology	2423
PLK1 (208G4) Rabbit mAb	Cell Signaling Technology	4513
PKCζ (C24E6) Rabbit mAb	Cell Signaling Technology	9368
PKR Antibody	Cell Signaling Technology	3072
p53 Antibody (D-11)	Santa Cruz Biotechnology	sc-17846
Nanog Antibody (1E6C4)	Santa Cruz Biotechnology	sc-293121
Nanog Antibody (A-11)	Santa Cruz Biotechnology	sc-374001
Nanog Antibody (M-17)	Santa Cruz Biotechnology	sc-30329
Nanog Antibody (C-4)	Santa Cruz Biotechnology	sc-376915
NUMB Antibody (P-20)	Santa Cruz Biotechnology	sc-15590
NUMB Antibody (48)	Santa Cruz Biotechnology	sc-136554
Notch 1 Antibody (C-10)	Santa Cruz Biotechnology	sc-373891
PKC zeta Antibody (H-1)	Santa Cruz Biotechnology	sc-17781
p-PKC ζ Antibody (H-2)	Santa Cruz Biotechnology	sc-271962
PKR Antibody (B-10)	Santa Cruz Biotechnology	sc-6282

PKR Antibody (M-515)	Santa Cruz Biotechnology	sc-1702
PKA alpha cat Antibody (C-20)	Santa Cruz Biotechnology	sc-903
beta-Actin Antibody (AC-15)	Santa Cruz Biotechnology	sc-69879
Chemicals, Peptides, and Recombinant Proteins		
aPKC- ζ pseudosubstrate inhibitor (PPI)	Tocris BioScience	1791
Phosphocellulose p81 paper	Millipore	20134
Hygromycin	InvivoGen	ant-hg-1
Geneticin	Gibco	10131035
Zeocin	Invitrogen	R25001
Blasticidin	InvivoGen	ant-bl-1
Tamoxifen	Sigma	T5648
Corn Oil	Sigma	C8267
Bromodeoxyuridine (BrdU)	BD Pharmingen	550891
Collagenase/Dispase	Roche	10269638001
MAX Efficiency DH5α Competent Cells	Tocris BioScience	18258-012
MasterAmp™ Taq DNA Polymerase	Epicentre	Q82000
Lieber-DeCarli Regular Control Rat Diet	Dyets inc	710027
Lieber-DeCarli Regular Control Rat Diet	Dyets inc	710362
Dulbecco's modified Eagle's medium (DMEM, high-glucose)	Corning	10-103
Fetal Bovine Serum (FBS)	Gibco	10438-026
100X Penicillin/Streptomycin	Genesee	25-512
L-Glutamine	Genesee	25-509
MEM non-essential amino acids	Corning	25-025
DPBS	Genesee	25-508
Trypsin-EDTA	Genesee	25-510X
LB Broth(Miller)	Sigma Aldrich	L3522
BioT	Bioland Scientific LLC	B01-01
100x Halt Protease Inhibitor Cocktail	Thermo Fisher Scientific	78430
Protein A/G PLUS-Agarose	Santa Cruz Biotechnology	sc-2003
MK-5108 (VX-689)	AdooQ	A11410
Hamster Fibronectin	Innovative Research	IHMFBN
Aurora-A	Millipore Ltd	14-511
Critical Commercial Assays		
Dual-Luciferase Reporter Assay System Kit	Promega	E1980
Omniscript RT kit	Qiagen	205113
MEGAshortscript™ Kit	Ambion	AM1354
QuikChange Lightning Site-Directed Mutagenesis Kit	Agilent Technologies	210519
West Pico Substrate solution kit	Thermo Fisher Scientific	34577
QIAprep Spin Miniprep Kit	QIAGEN	27106
mMESSAGE mMACHINE T7 ULTRA Transcription Kit	Ambion	AM1345
MiRNA Northern Blot Assay Kit	Signosis	NB-0001
Kinase Assay Kit	SignalChem	P75-10G

Experimental Models: Cell Lines		
Human: Huh7		
Human: HepG2		
Human: Primary Hepatocytes		
Mouse: Primary Hepatocytes		
Experimental Models: Organisms/Strains		
Mouse: *Alb-CreERT2*	Gift from Dr. Daniel Metzger and Pierre Chambon, IGBM, Illkirch, France	N/A
Mouse: *Ns5aTg*	Gift from Dr. Ratna Ray (Saint Louis Univ.)	N/A
Mouse: *Numb-3A*$^{LSL-3A}$	This paper	N/A
Mouse: *Tbc1d15*$^{Flox/Flox}$	This paper	N/A
Oligonucleotides		
Genotyping primer: NUMB3A Forward CCTTATGACGTGCCTGACTATG	This paper	N/A
Genotyping primer: NUMB3A Reverse CATTCCTTCTCCCGCTTCTG	This paper	N/A
Genotyping primer: HCV-NS5A Forward GGACGATGAGGATCGTCGG	This paper	N/A
Genotyping primer: HCV-NS5A Reverse GCTAGCCGAGGAGCTGG	This paper	N/A
Genotyping primer: TBC1D15-Flox Forward CATGTGAAGGATCACAGAGTAGG	This paper	N/A
Genotyping primer: TBC1D15-Flox Reverse AGCTGGGTTTGTTTAGGTAAGA	This paper	N/A
Genotyping primer: TBC1D15-WT Forward CTTGATGAACCAGCATATGGC	This paper	N/A
Genotyping primer: TBC1D15-WT Reverse CACAACGGGTTCTTCTGTTAGTCC	This paper	N/A
Genotyping primer: CreER2 Forward ATGCTTCTGTCCGTTTGCCG	This paper	N/A
Genotyping primer: CreER2 Reverse CCTGTTTTGVACGTTCACCG	This paper	N/A
q-PCR primer: (Hu) p53 Forward AGGGATGTTTGGGAGATGTAAG	[9]	N/A
q-PCR primer: (Hu) p53 Reverse CCTGGTTAGTACGGTGAAGTG	[9]	N/A
q-PCR primer: (Hu) Nanog Forward AATACCTCAGCCTCCAGCAGA	[7]	N/A
q-PCR primer: (Hu) Nanog Reverse TGCGTCACACCATTGCTATTC	[7]	N/A
q-PCR primer: (Ms) Nanog Forward CATGTGGTTGCTGGGATTTG	[7]	N/A

q-PCR primer: (Ms) Nanog Reverse GTGAGATGGCTCAGTGGATAAG	[7]	N/A
Recombinant DNA		
Full Length mTBC1D15-FLAG-HA	[9]	N/A
mTBC1D15 N-Terminus-FLAG-HA	[9]	N/A
mTBC1D15 C-Terminus-FLAG-HA	[9]	N/A
mTBC1D15-N-2KR-myc-HA	[9]	N/A
mTBC1D15-CΔC-myc-HA	[9]	N/A
Full Length mTBC1D15-myc-HA	[9]	N/A
mTBC1D15- $N_{1/2}$-GFP	[9]	N/A
mTBC1D15- N_{cno}-GFP	[9]	N/A
shTBC1D15-685	[9]	N/A
shTBC1D15-963	[9]	N/A
hNOTCH1-Full Length (no tag)	This paper	N/A
hNOTCH1-Full Length-myc	Dr. Chengyu Liang	human full-length Notch is expected to be 2555 aa: ~210kd
hNOTCH1-ΔE-myc	Dr. Chengyu Liang	full-length Notch with the deletion of extracellular domain after S2 cleavage around 1720; so 2555-1720= 835aa: ~130kd
hNOTCH1-TMRM-myc	Dr. Chengyu Liang	TMEM contains TM + RAM= 20-100=120aa: ~15kd
hNOTCH1-ΔE-ΔRAM -myc	Dr. Chengyu Liang	the RAM is about 100aa (1757-1857aa); this is 835-100=735: ~125kd
hNOTCH1 ΔE V1754L-myc	Dr. Chengyu Liang	(S3 cleavage site mutant): this one is similar to ΔE: 835AA: ~130kd: This is the intracellular domain with early stop codon at PEST domain.
hNOTCH1-ICD-FLAG-HA	Dr. Chengyu Liang	this is intracellular part after S3 cleavage, thus should be 2555-1754= 801: ~110kd
hNOTCH1-ICD-Δ82-FLAG-HA	Dr. Chengyu Liang	(deletion of PAS domain: which mimic human patient early stop codon); this is NICD-C-terminal PEST domain 82 aa = 801-82=719aa: ~95kd: This is the intracellular domain with early stop codon at PEST domain. 2473aa-2555aa

hNOTCH1-ICD-Δ162-FLAG-HA	Dr. Chengyu Liang	(deletion of PAS domain: which mimic human patient early stop codon): This one should be 801-162=639aa: ~80kd: This is the intracellular domain with early stop codon at PEST domain. 2393aa-2555aa
p-3X-Flag-HA-Numb-3A	Dr. Kaibuchi	N/A
Numb4-eGFP-M107K	Addgene	37805
pRL-cMYC-3UTR-Luc	Addgene	4081
TRC2-pLKO-shTbc1d15 (4 Plasmids)	Sigma	TRCN0000250021250021-25
TRC2-pLKO-shTbc1d15 (4-plasmids)	Sigma	TRCN0000231963-66
TRC-pLKO.1-shMSI2 (4 plasmids)	Sigma	TRCN000062809-12
TRC-pLKO.1-shMsi2 (4 plasmids)	Sigma	TRCN0000073-77
pLentGIIICMV-TBCD15-GFP-2A-Puro	Abm Good	LV329564
pLenti-GIII-CMV-RFP-2A-Puro	Abm Good	LV228929
pLenti-GIII-CMV-GFP-2A-Puro	Abm Good	LV423599
Cas9 nuclease expression Clone	GeneCopoeia	CP-C9NU-01
SgRNA Clone for ROSA26 gene	GeneCopoeia	HCP02111-SG01
Custom Designed Donor Plasmid	GeneCopoeia	DOR02111
pluc-Hey1	[39]	N/A
pluc-Hey1-Δ215	[39]	N/A
RPBJ-mutB	[39]	N/A
pGL-BASIC	[39]	N/A
pluc-ΔSacI/HindIII	[39]	N/A
plucΔ41	[39]	N/A
PGI3-Hey2	[39]	N/A
Software and Algorithms		
GraphPad Prism 6	GraphPad Software	https://www.graphpad.com/scientific-software/prism/
ImageJ	N/A	https://imagej.nih.gov/ij/
Proteome Discoverer 1.4, Sequest algorithms	Thermo Fisher Scientific	https://www.thermofisher.com/order/catalog/product/OPTON-30795
ProSightPC™ Software	Thermo Fisher Scientific	https://www.thermofisher.com/order/catalog/product/PROSIGHTPC10
RPBJ-mutB	[39]	N/A
Deposited DatapGL-BASIC	[39]	N/A
Human Gene expression profiling by arraypluc-ΔSacI/HindIII	[39, 40]	GSE17856N/A
Human Gene expression profiling by arraypluc-Δ41	[39]	GSE27150N/A
PGI3-Hey2	[39]	N/A
Software and Algorithms		

GraphPad Prism 6	GraphPad Software	https://www.graphpad.com/scientific-software/prism/
ImageJ	N/A	https://imagej.nih.gov/ij/
Proteome Discoverer 1.4, Sequest algorithms	Thermo Fisher Scientific	https://www.thermofisher.com/order/catalog/product/OPTON-30795
ProSightPC™ Software	Thermo Fisher Scientific	https://www.thermofisher.com/order/catalog/product/PROSIGHTPC10
Deposited Data		
Human Gene expression profiling by array	[40]	GSE17856
Human Gene expression profiling by array		GSE27150

a

Creation of Conditional Knock out mose Tbc1d15 - IKMC Project: 45640 (IKMC-International Knockout Mouse Consortium:

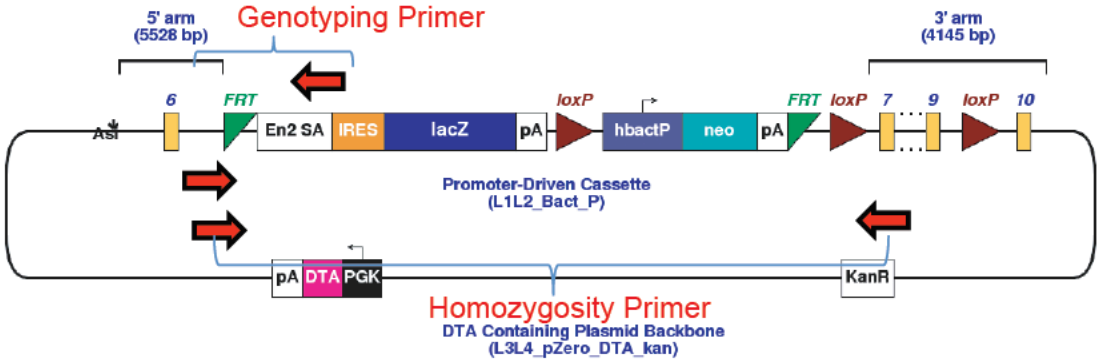

Genotyping primer Sequences:(Red sequences exon 6 of TBC1d15 and LAR3 primer sequences; LAR3 reverse primer)

b

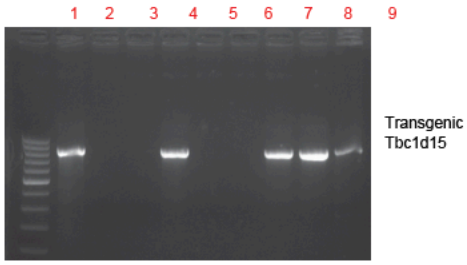

c

Genotyping primer Sequences:(Red sequences exon 6 of TBC1d15 and Exon7 primer sequences)

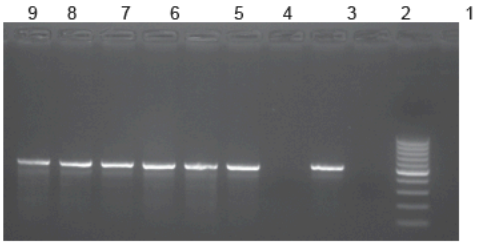

Homozygous for Transgenic Tbc1d15: Mouse 1 & 3

Supplementary Fig. 1
Choi and Siddique al.

Supplemental Figures:

Supplementary Figure 1. Creation of conditional knockout mouse of Tbc1d15 from International Knockout Mouse Consortium (IKMC Project # 45640).

(**a**) Pictorial diagram shows the construction of Tbc1d15 plasmid backbone for transgenic mouse and plasmid map. (**b**). Pictorial diagram shows the Tbc1d15 genotyping. Genotyping primer Sequences: (Forward primer sequences were from Exon 6 of Tbc1d15 and reverse primer

was from LAR3 sequences. This genotyping is shown from three independent experiments. (**c**) Pictorial diagram shows the homozygosity. For homozygosity primer Sequences were synthesized from Exon 6 of Tbc1d15 and Exon7 primer. This genotyping is shown from three independent experiments.

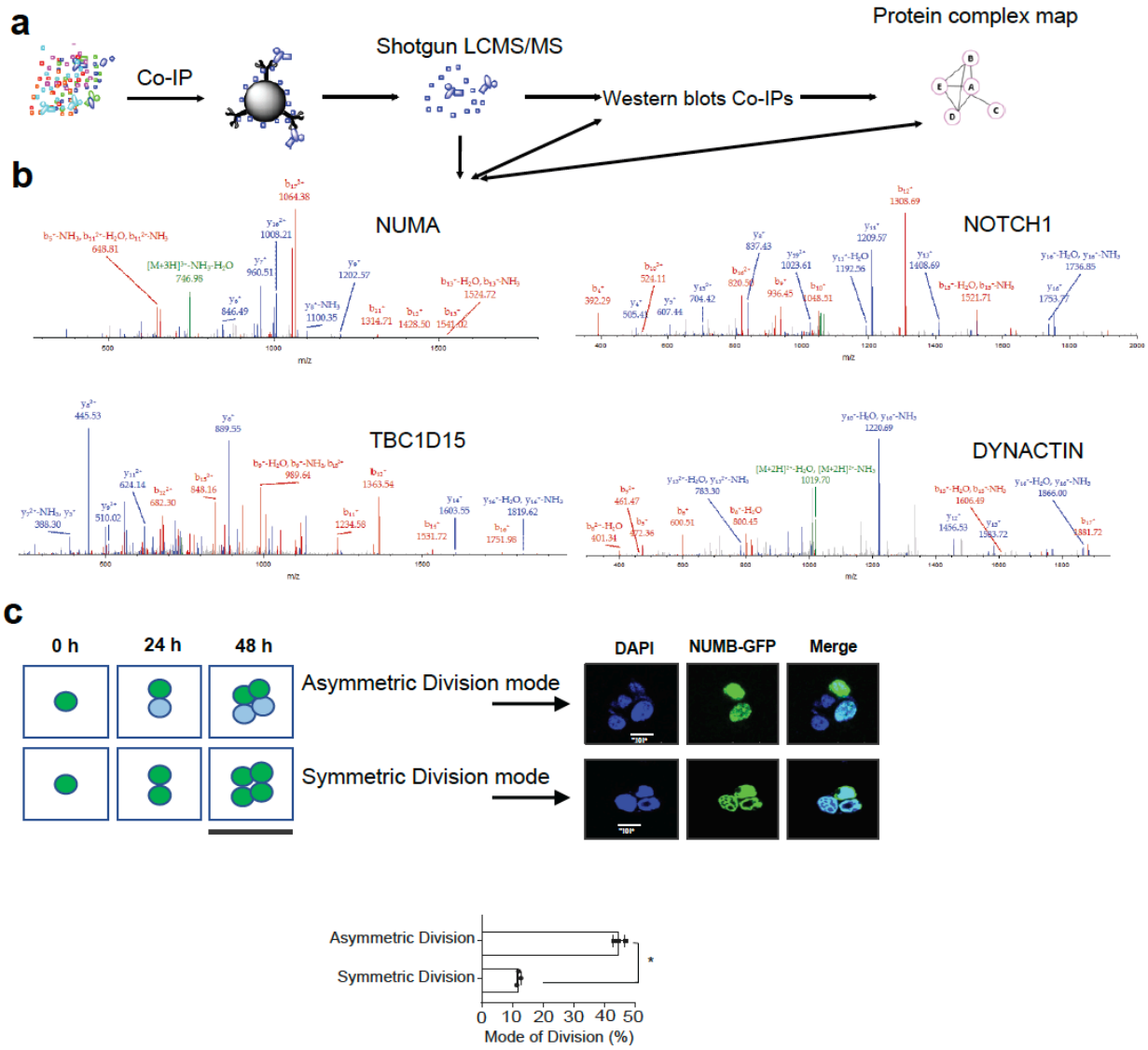

Supplementary Fig. 2
Choi and Siddique et al.

Supplementary Figure 2. The protein complex was isolated from cell lysate by antibody immunoprecipitation.

(**a**) Enriched protein complexes were divided into two parts for shotgun proteomics experiment and Western blots Co-IPs. (**b**) Representative mass spectra of target proteins in the protein complex. Proteins are digested enzymatically to peptides by trypsin, leading to peptides with C-terminally protonated amino acids, the peptides are separated by HPLC and sequenced by high resolution MS/MS. The MS and MS/MS spectra were acquired and matched against protein sequence databases. The outcome of the experiment was the identity of the peptides and therefore the proteins making up the protein complex. (**c**) Asymmetric vs. symmetric cell division analyses. Data are represented as ±SD (n=3). p-values by two-tailed unpaired t test. *p<0.05 (Student's t test).

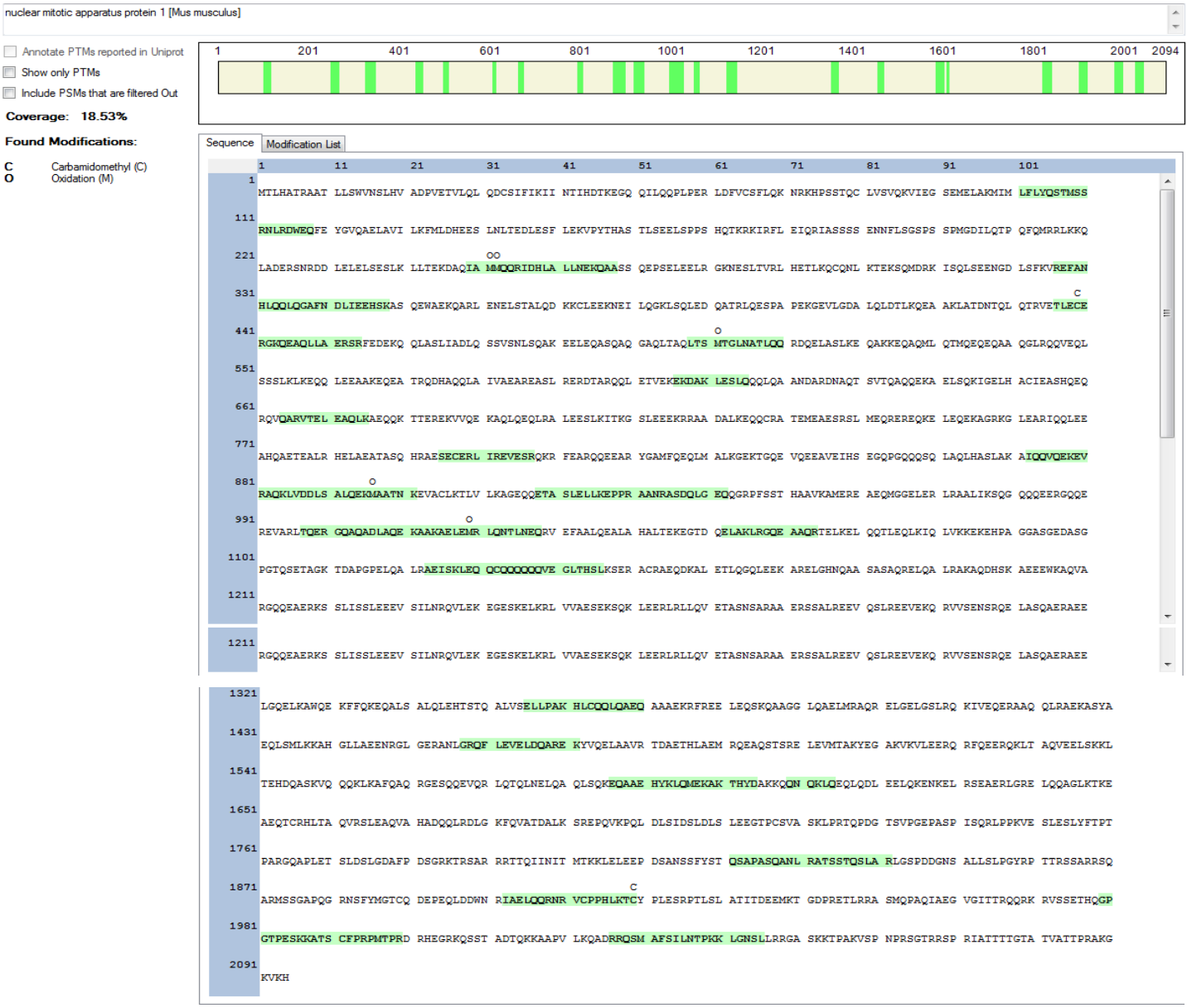
nuclear mitotic apparatus protein 1 [Mus musculus]
Annotate PTMs reported in Uniprot
Show only PTMs
Include PSMs that are filtered Out
Coverage: 18.53%
Found Modifications:
C Carbamidomethyl (C)
O Oxidation (M)
1 201 401 601 801 1001 1201 1401 1601 1801 2001 2094
Sequence
Modification List
1 11 21 31 41 51 61 71 81 91 101
1 MTLHATRAAT LLSWVNSLHV ADPVETVLQL QDCSIFIKII NTIHDTKEGQ QILQQPLPER LDFVCSFLQK NRKHPSSTQC LVSVQKVIEG SEMELAKMIM LFLVQSTMSS
111 RNLRDWEQFE YGVQAELAVI LKFMLDHEES LNLTEDLESF LEKVPYTHAS TLSEELSPPS HQTKRKIRFL EIQRIASSSS ENNFLSGSPS SPMGDILQTP QFQMRRLKKQ
221 LADERSNRDD LELELSESLK LLTEKDAQIA MMQQRIDHLA LLNEKQAASS QEPSELEELR GKNESLTVRL HETLKQCQNL KTEKSQMDRK ISQLSEENGD LSFKVREFAN
331 HLQQLQGAFN DLIEEHSKAS QEWAEKQARL ENELSTALQD KKCLEEKNEI LQGKLSQLED QATRLQESPA PEKGEVLGDA LQLDTLKQEA AKLATDNTQL QTRVETLECE
441 RGKQEAQLLA ERSRFEDEKQ QLASLIADLQ SSVSNLSQAK EELEQASQAQ GAQLTAQLTS MTGLNATLQQ RDQELASLKE QAKKEQAQML QTMQEQEQAA QGLRQQVEQL
551 SSSLKLKEQQ LEEAAKEQEA TRQDHAQQLA IVAEAREASL RERDTARQQL ETVEKEKDAK LESLQQQLQA ANDARDNAQT SVTQAQQEKA ELSQKIGELH ACIEASHQEQ
661 RQVQARVTEL EAQLKAEQQK TTEREKVVQE KAQLQEQLRA LEESLKITKG SLEEEKRRAA DALKEQQCRA TEMEAESRSL MEQREREQKE LEQEKAGRKG LEARIQQLEE
771 AHQAETEALR HELAEATASQ HRAESECERL IREVESRQKR FEARQQEEAR YGAMFQEQLM ALKGEKTGQE VQEEAVEIHS EGQPGQQQSQ LAQLHASLAK AIQQVQEKEV
881 RAQKLVDDLS ALQEKMAATN KEVACLKTLV LKAGEQQETA SLELLKEPPR AANRASDQLG EQQGRPFSST HAAVKAMERE AEQMGGELER LRAALIKSQG QQQEERGQQE
991 REVARLTQER GQAQADLAQE KAAKAELEMR LQNTLNEQRV EFAALQEALA HALTEKEGTD QELAKLRGQE AAQRTELKEL QQTLEQLKIQ LVKKEKEHPA GGASGEDASG
1101 PGTQSETAGK TDAPGPELQA LRAEISKLEQ QCQQQQQQVE GLTHSLKSER ACRAEQDKAL ETLQGQLEEK ARELGHNQAA SASAQRELQA LRAKAQDHSK AEEEWKAQVA
1211 RGQQEAERKS SLISSLEEEV SILNRQVLEK EGESKELKRL VVAESEKSQK LEERLRLLQV ETASNSARAA ERSSALREEV QSLREEVEKQ RVVSENSRQE LASQAERAEE
1211 RGQQEAERKS SLISSLEEEV SILNRQVLEK EGESKELKRL VVAESEKSQK LEERLRLLQV ETASNSARAA ERSSALREEV QSLREEVEKQ RVVSENSRQE LASQAERAEE
1321 LGQELKAWQE KFFQKEQALS ALQLEHTSTQ ALVSELLPAK HLCQQLQAEQ AAAEKRFREE LEQSKQAAGG LQAELMRAQR ELGELGSLRQ KIVEQERAAQ QLRAEKASYA
1431 EQLSMLKKAH GLLAEENRGL GERANLGRQF LEVELDQARE KYVQELAAVR TDAETHLAEM RQEAQSTSRE LEVMTAKYEG AKVKVLEERQ RFQEERQKLT AQVEELSKKL
1541 TEHDQASKVQ QQKLKAFQAQ RGESQQEVQR LQTQLNELQA QLSQKEQAAE HYKLQMEKAK THYDAKKQQN QKLQEQLQDL EELQKENKEL RSEAERLGRE LQQAGLKTKE
1651 AEQTCRHLTA QVRSLEAQVA HADQQLRDLG KFQVATDALK SREPQVKPQL DLSIDSLDLS LEEGTPCSVA SKLPRTQPDG TSVPGEPASP ISQRLPPKVE SLESLYFTPT
1761 PARGQAPLET SLDSLGDAFP DSGRKTRSAR RRTTQIINIT MTKKLELEEP DSANSSFYST QSAPASQANL RATSSTQSLA RLGSPDDGNS ALLSLPGYRP TTRSSARRSQ
1871 ARMSSGAPQG RNSFYMGTCQ DEPEQLDDWN RIAELQQRNR VCPPHLKTCY PLESRPTLSL ATITDEEMKT GDPRETLRRA SMQPAQIAEG VGITTRQQRK RVSSETHQGP
1981 GTPESKKATS CFPRPMTPRD RHEGRKQSST ADTQKKAAPV LKQADRRQSM AFSILNTPKK LGNSLLRRGA SKKTPAKVSP NPRSGTRRSP RIATTTTGTA TVATTPRAKG
2091 KVKH

Sequence: LFLYQSTMSSRNLRDWEQ, Charge: +3, Monoisotopic m/z: 758.71967 Da

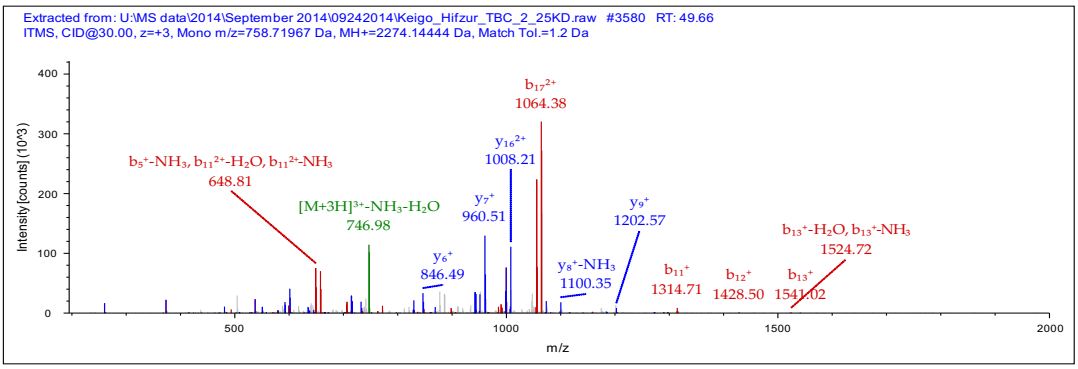

Sequence: ELLPAKHLCQQLQAEQ, Charge: +2, Monoisotopic m/z: 924.96918 Da

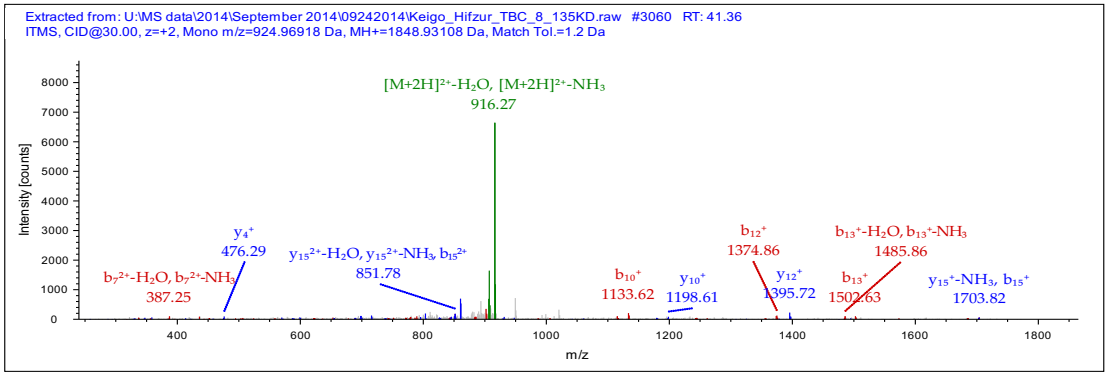

Sequence: REFANHLQQLQGAFNDLIEEHSK, Charge: +3, Monoisotopic m/z: 908.79010 Da

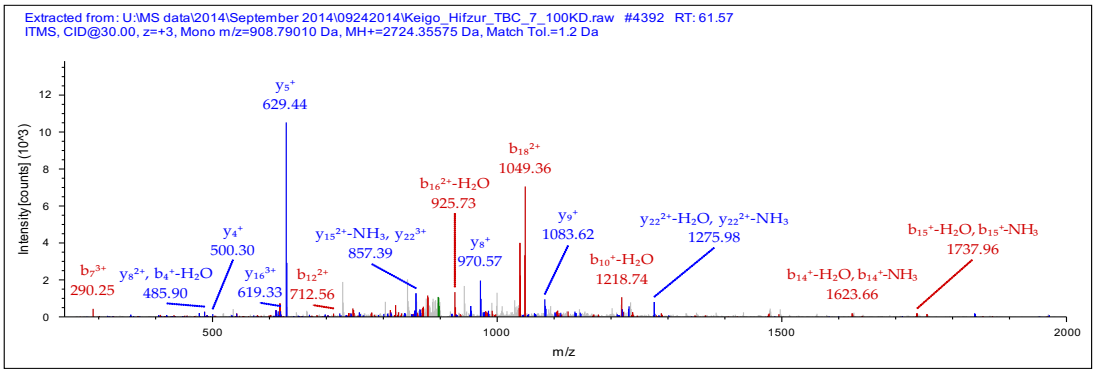

5

Sequence: KLEQQCQQQQQQVEGLTHSL, Charge: +2, Monoisotopic m/z: 1177.03430 Da

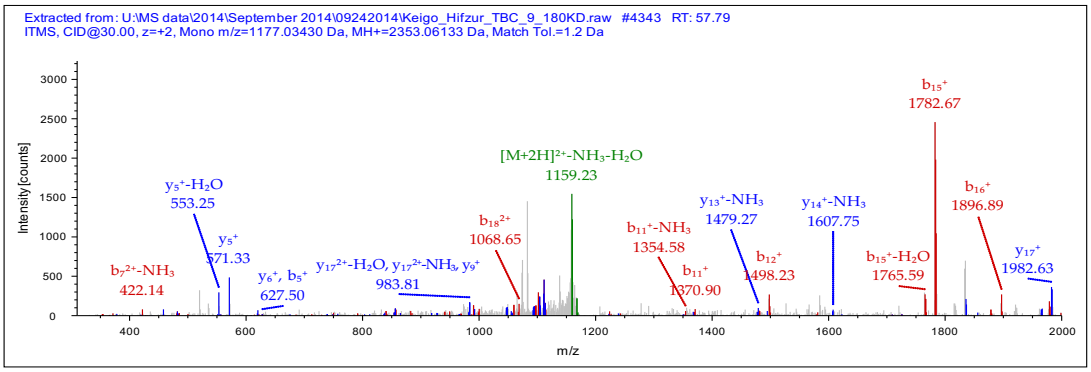

Sequence: GPGTPESKKATSCFPRPMTPR, Charge: +2, Monoisotopic m/z: 1123.02637 Da

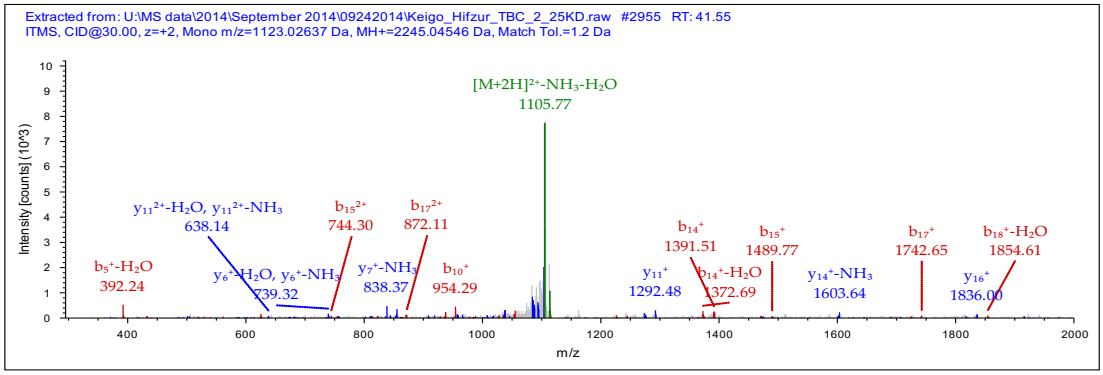

Sequence: TLECERGKQEAQLLAERSR, C4-Carbamidomethyl (57.02146 Da)
Charge: +2, Monoisotopic m/z: 1137.57263 Da

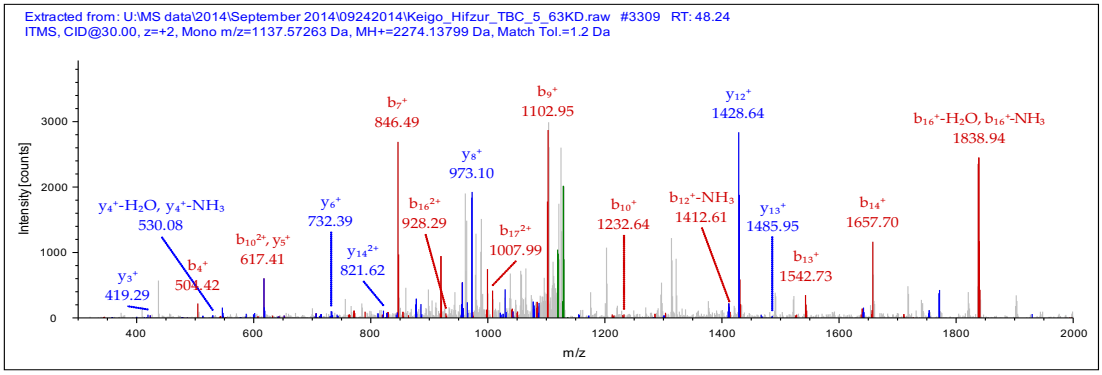

Sequence: EMRLQNTLNEQ, Charge: +2, Monoisotopic m/z: 688.36584 Da

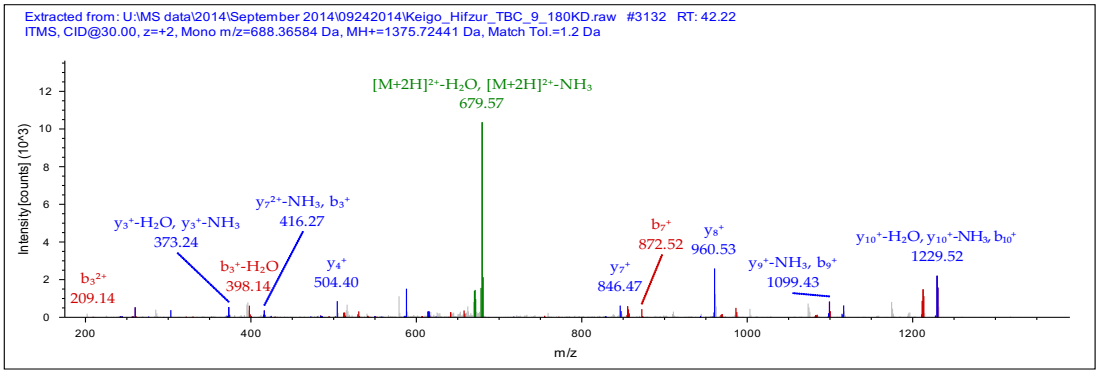

Sequence: EKDAKLESLQ, Charge: +2, Monoisotopic m/z: 580.82843 Da

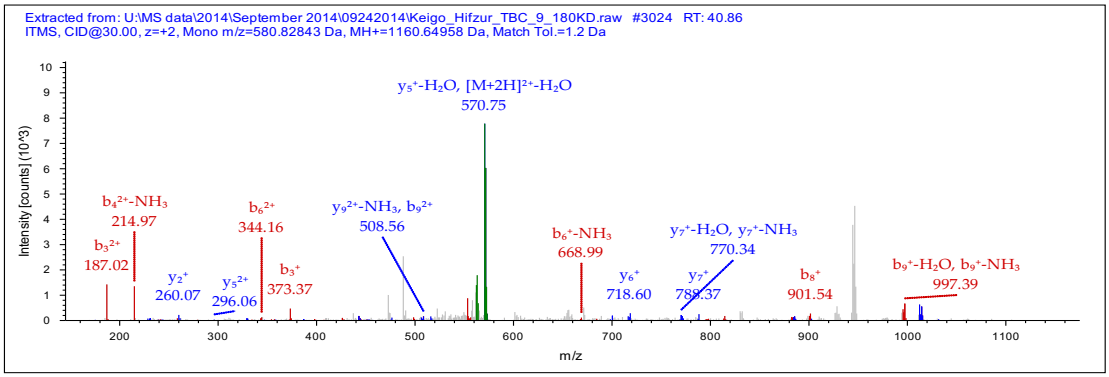

Sequence: ELAKLRGQEAAQR, Charge: +2, Monoisotopic m/z: 735.42499 Da

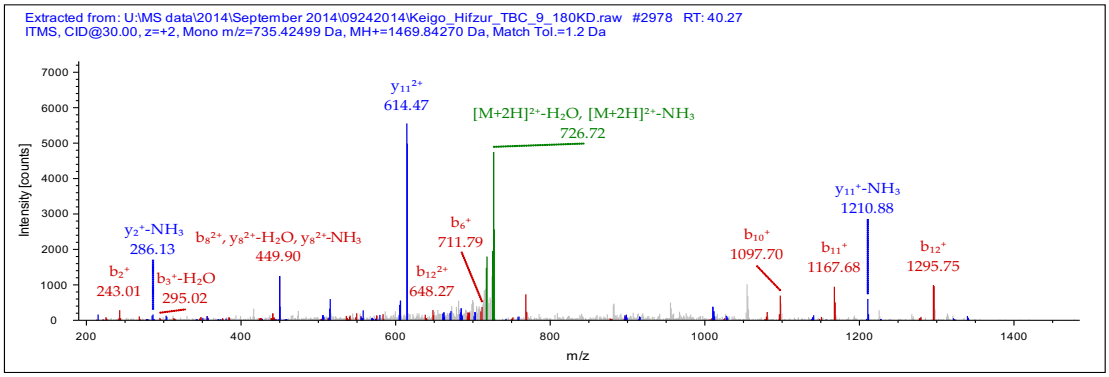

5

Sequence: SECERLIREVESR, Charge: +2, Monoisotopic m/z: 803.41425 Da

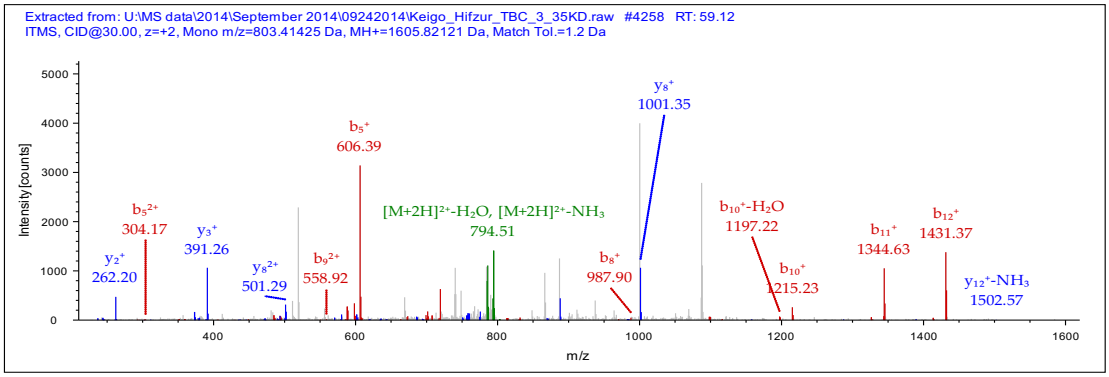

Sequence: LTSMTGLNATLQQ, M4-Oxidation (15.99492 Da)

Charge: +2, Monoisotopic m/z: 697.36707 Da

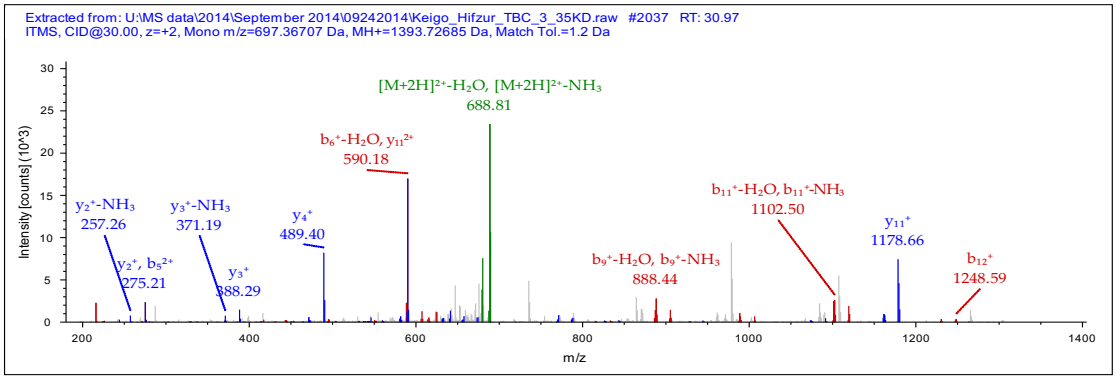

Sequence: QNQKLQ, Charge: +2, Monoisotopic m/z: 379.72855 Da

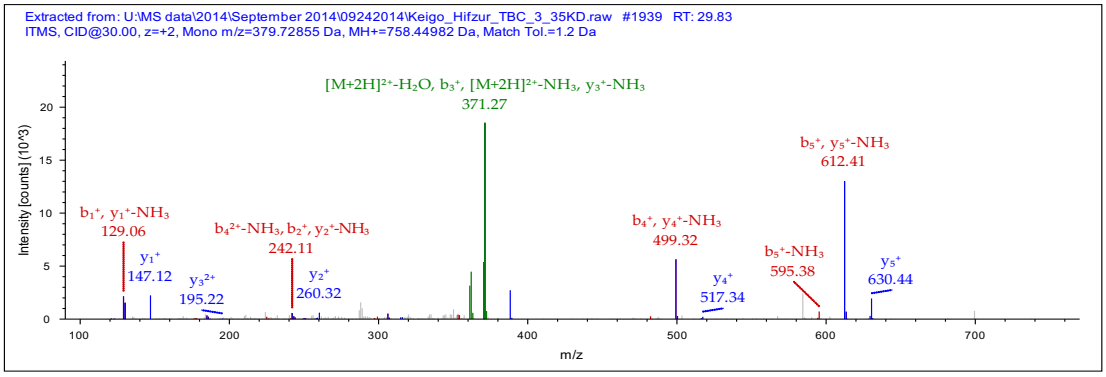

Sequence: IAELQQRNRVCPPHLKTC, C18-Carbamidomethyl (57.02146 Da)
Charge: +2, Monoisotopic m/z: 1082.03015 Da

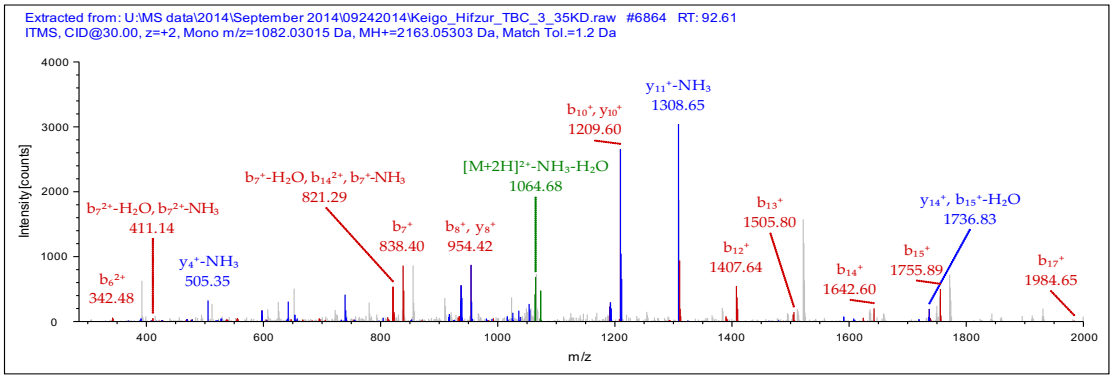

Sequence: RRQSMAFSILNTPKKLGNSL, Charge: +2, Monoisotopic m/z: 1131.07996 Da

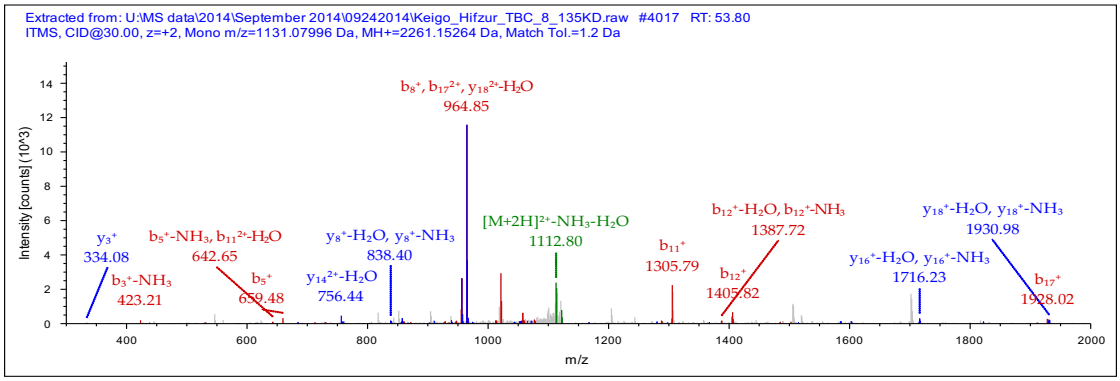
Extracted from: U:\MS data\2014\September 2014\09242014\Keigo_Hifzur_TBC_8_135KD.raw #4017 RT: 53.80
ITMS, CID@30.00, z=+2, Mono m/z=1131.07996 Da, MH+=2261.15264 Da, Match Tol.=1.2 Da
Intensity [counts] (10^3)
m/z
b8+, b17 2+, y18 2+-H2O
964.85
[M+2H]2+-NH3-H2O
1112.80
b12+-H2O, b12+-NH3
1387.72
y18+-H2O, y18+-NH3
1930.98
y3+
334.08
b5+-NH3, b11 2+-H2O
642.65
y8+-H2O, y8+-NH3
838.40
b11+
1305.79
y16+-H2O, y16+-NH3
1716.23
b3+-NH3
423.21
b5+
659.48
y14 2+-H2O
756.44
b12+
1405.82
b17+
1928.02

Supplementary Figure 3. Mass-spectrometry data of NuMA1 protein that binds TBC1D15. Representative mass spectra of NuMA1 proteins in the protein complex is shown above. Proteins are digested enzymatically to peptides by trypsin, leading to peptides with C-terminally protonated amino acids, the peptides are separated by HPLC and sequenced by high resolution MS/MS. The MS and MS/MS spectra were acquired and matched against protein sequence databases. The outcome of the experiment was the identity of the peptides and therefore the proteins making up the protein complex.

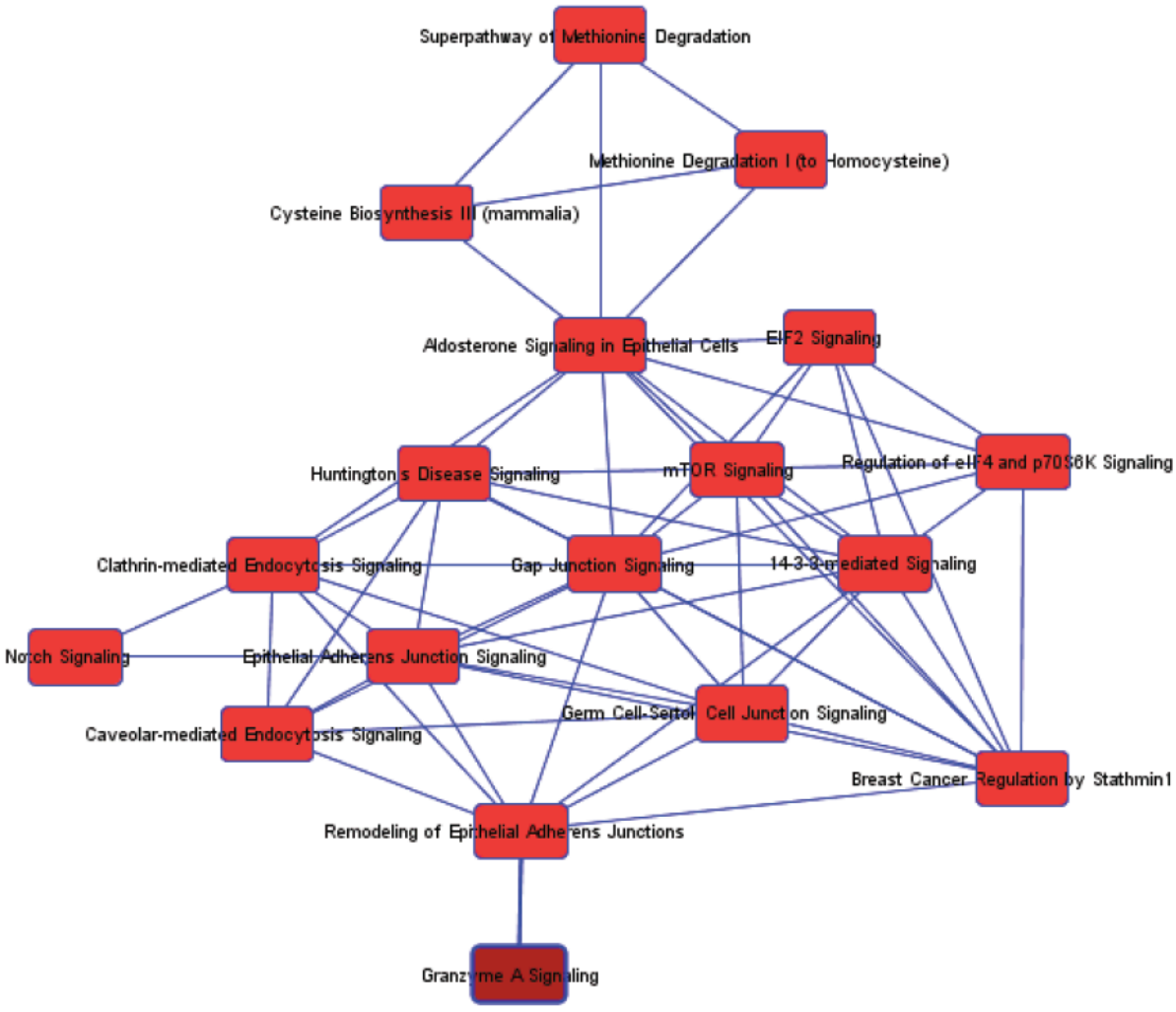

Supplementary Fig. 4
Choi and Siddique et al.

Supplementary Figure 4. Canonical Pathway analysis for the identified proteins. Pathway analysis was performed to identify the inks of these pathways that were found in IP-Mass-spec analyses of TBC1D15-binding proteins. Note that NOTCH pathway is linked to endocytosis and adhesion-junction pathways.

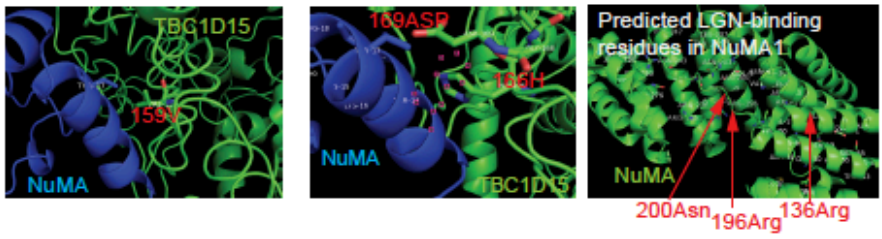

Supplementary Fig. 5
Choi and Siddique *et al.*

Supplementary Figure 5. The 169ASP residue of TBC1D15 (green) interacts with NuMA1 (blue). To visualize the interaction between full-length TBC1D15 and C-terminus of NuMA1, occluding portions of TBC1D15 were not included in the simulation. Docking conformations were ranked according to lowest free energy of calculated structures. The docking of NUMA1 was the best candidate from this analysis and highlights the importance of this residue in mediating the interaction between the N-terminal region (aa 1-270) of TBC1D15 and NUMA1.

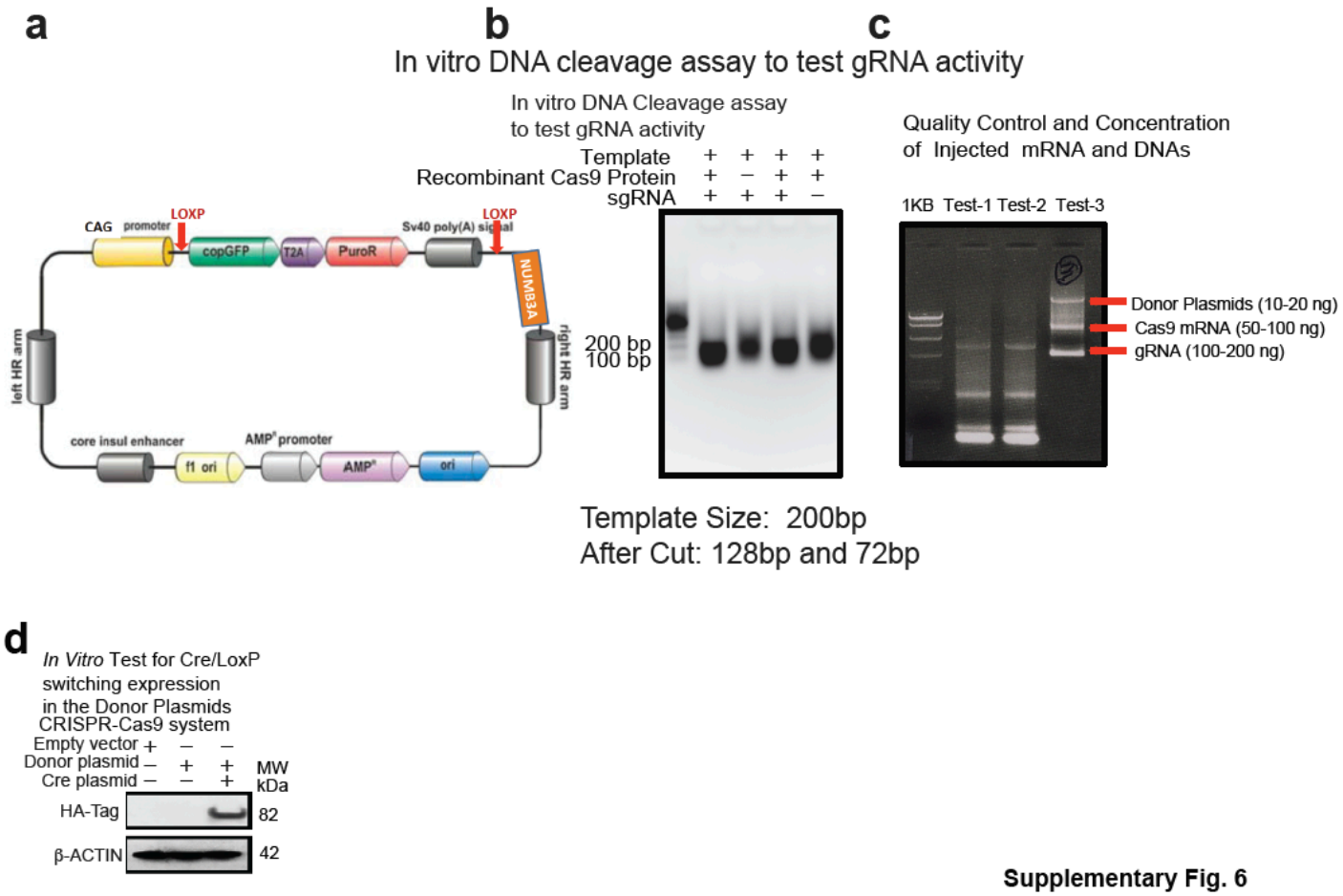

Supplementary Fig. 6
Choi and Siddique et al.

Supplementary Figure 6. Construction of donor plasmid and subsequent quality control analysis.

(**a**) Pictorial diagram shows the Donor plasmid for knocking in the customer-specified, inducible transgene to the mouse safe Harbor (Rosa26) locus. Total Plasmid Size: 11764 bp (vector: ROSA26). The sequences were arranged in the following sequences- 5'arm Rosa 26- SA-CAG promoter-LoxP-EF1a- CopGFP-T2A- Puro- SV40 poly(A) signal -LoxP-Kozak-ATG-HA-NUMB-3A-Stop codon-pA (terminator)-3' arm of Rosa 26 locus. (**b**) Pictorial diagram shows *In vitro* DNA Cleavage assay to test gRNA activity. 600ng of Cas9 protein, 250ng gRNA, and 400ng of template containing a target sequences were incubated at 37˚C for 1hr. After treating with RNAse, the reaction mixture was analyzed in agarose gel. Template Size: 200bp (synthesized from IDT, USA). The successful cut produced two ladders of 128bp and 72bp. This *in vitro* DNA cleavage assay is shown from three independent experiments. (**c**) The gel picture shows the quality control and concentration of injected mRNA and DNAs. The representative pictures are shown from three independent experiments. (**d**) Immunoblots of *in vitro* test for Cre/LoxP switching expression in the Donor plasmids CRISPR-Cas9 system. The immunoblots analysis are shown from three independent experiments.

a

Description: Donor plasmid for knocking in the customer-specified, inducible transgene described above to the mouse Safe Harbor (Rosa26) locus
Whole Plasmid Size: 11764 bp
Vector: ROSA26

DONOR DRAWING:
5'arm Rosa 26- SA-CAG promoter-LoxP-EF1a- CopGFP-T2A- Puro- SV40 poly(A) signal -LoxP-Kozak-ATG-HA-NUMB-3A-Stop codon--pA (terminator)-3' arm of Rosa 26 locus

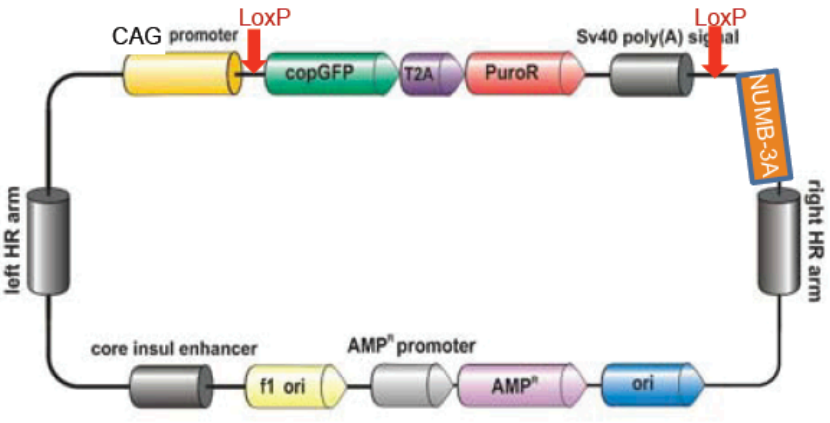

Chromosome and Left Hand Arm SPECIFIC PRIMER; Product length: 1046bp

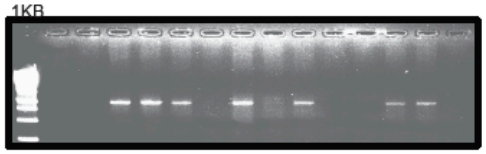

b

Chromosome and Right Hand Arm SPECIFIC PRIMER; Product length:

This is the proof for right insertion

c

HA-Tag SPECIFIC PRIMER; Product length:

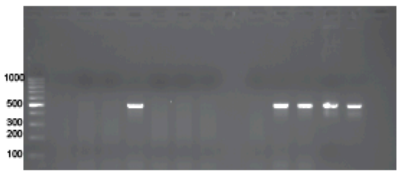

Supplementary Fig. 7
Choi and Siddique et al.

Supplementary Figure 7. This is the proof for right insertion of the NUMB-3A sequences. (**a**) The Gel picture shows the correct left insertion of the Knock in sequences. The chromosome and Left-Hand Arm (LHA) specific primers were designed and PCR was performed; Product length: 1046bp (**b**) The Gel picture shows the correct right insertion of the Knock in sequences.

The chromosome and Right-Hand Arm (RHA) specific primers were designed and PCR was performed; Product length: 1145bp. (**c**) The Gel picture shows the correct NUMB-3A sequences. The presence of NUMB-3A was assessed by designing the forward primer HA-Tag specific and Reverse primer from NUMB specific primer; Product length: 518bp. The representative pictures are shown from three independent experiments (**b, c**).

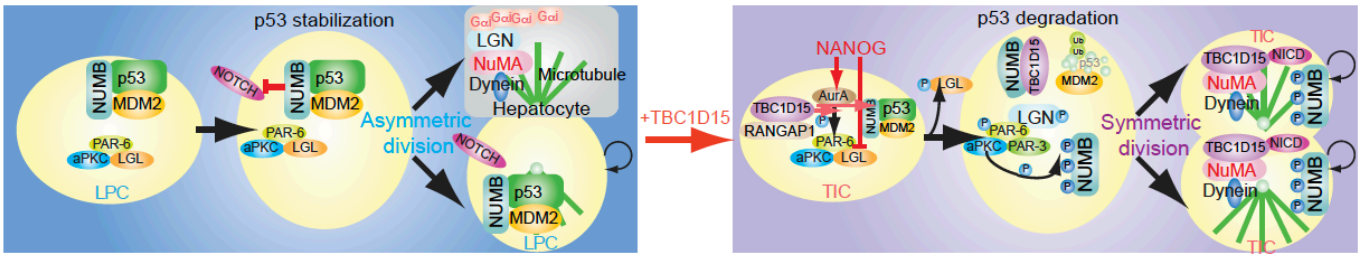

Supplementary Fig. 8
Choi and Siddique et al.

Supplementary Figure 8. Hypothetical model of TBC1D15-mediated NOTCH degradation and inhibition of asymmetric cell division and oncogenesis. (**Left**) Liver progenitor cells (LPC) undergo asymmetric cell division via establishment of asymmetric cell division machinery to bridge between microtublues and asymmetrically-dividing daughter cells through interactions of Gα-LGN-Dynein-Microtubules. (**Right**) The binding of N-terminus of TBC1D15 to NUMB promotes dissociation and proteolysis of p53 and phosphorylation of NUMB by cooperation of RANGAP1-TBC1D15 interactions. TLR4-NANOG axis promotes phosphorylation of NUMB and TBC1D15-mediated p53 degradation, leading to the genesis of TICs and liver oncogenesis in alcoholic liver disease. NuMA1-TBC1D15 interaction inhibits interactions between LGN-NuMA1 that is essential to establish asymmetric cell division machinery, leading to unrestricted expansion of stem cell compartment without differentiation (asymmetric cell division), leading to genesis of TICs, ultimately leading to recurrence and metastasis of hepatocellular carcinomas (HCCs).

Supplementary Figure 9. Uncropped film figures.

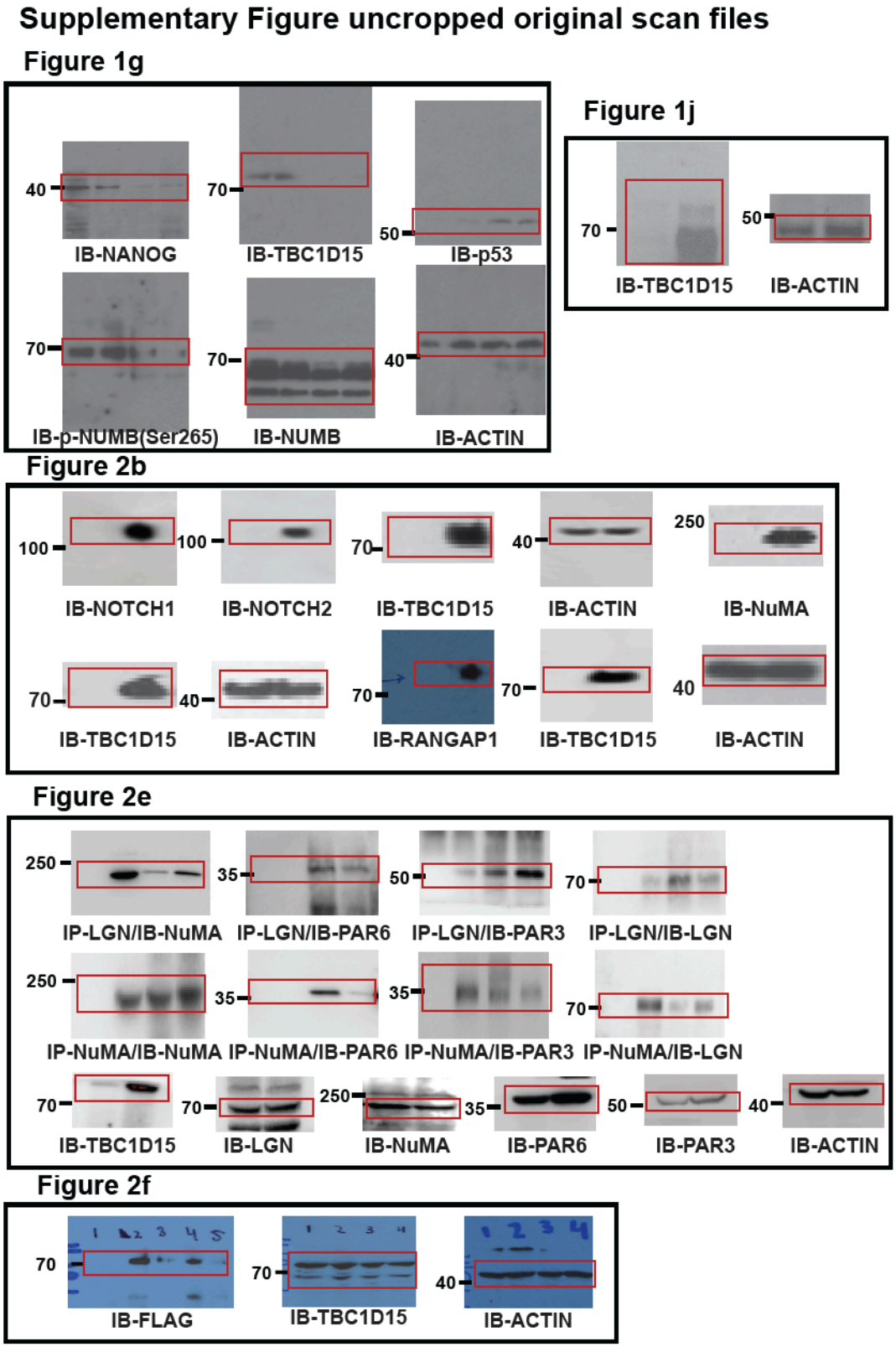

Figure 2g

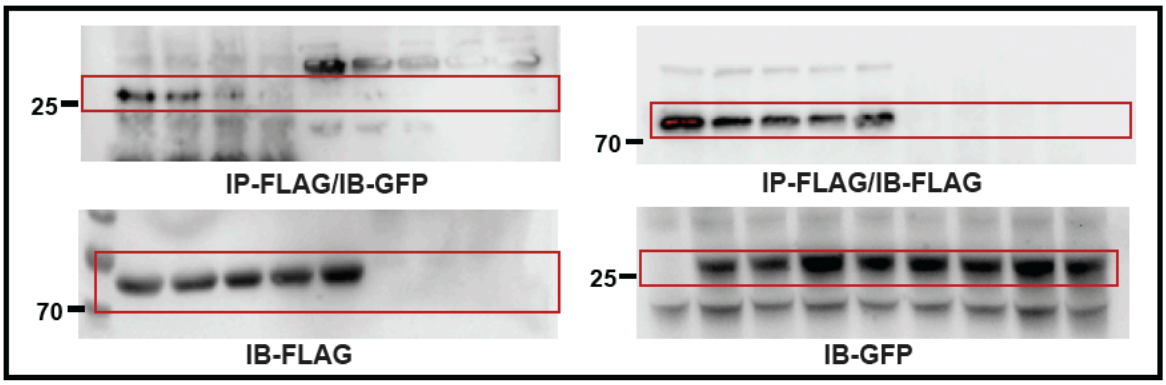

Figure 3b

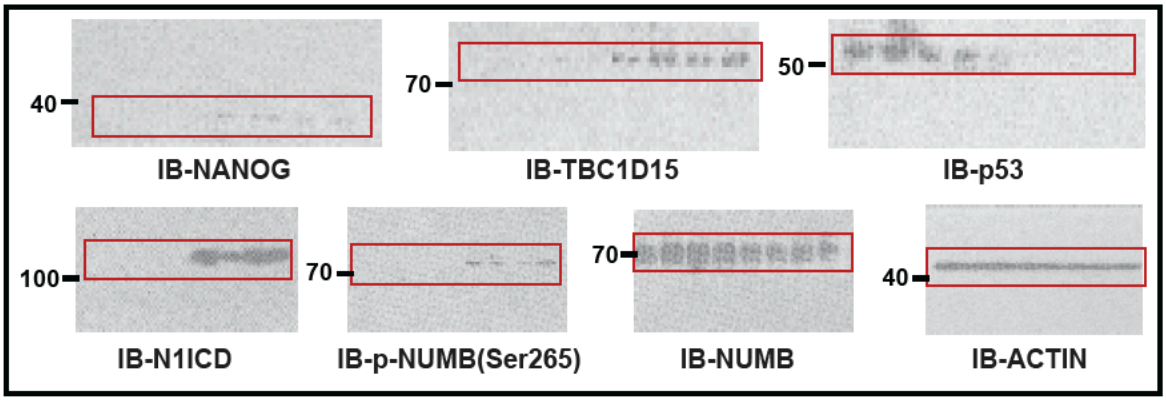

Figure 3d

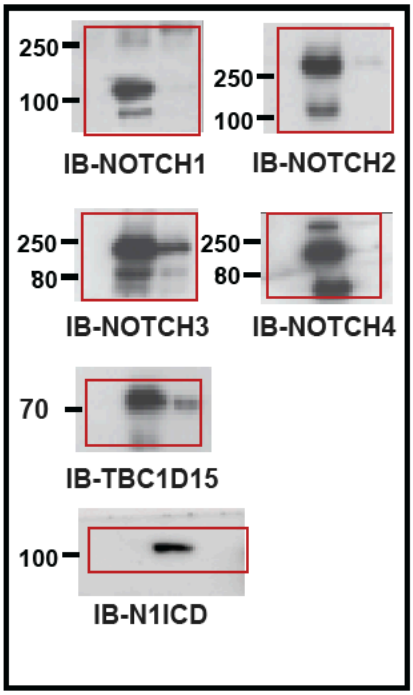

Figure 3e

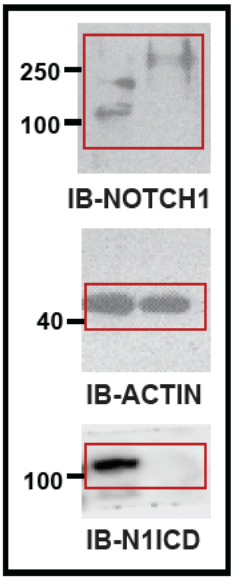

Figure 3f

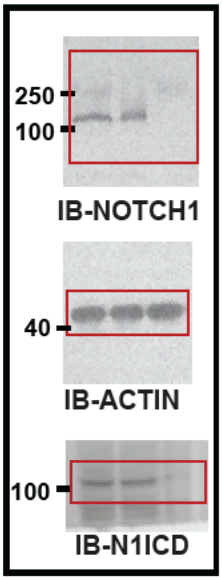

Figure 3g

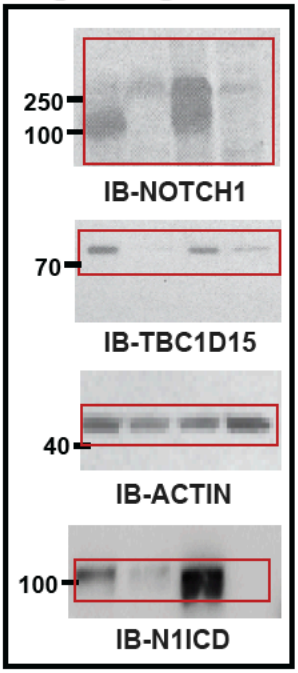

Figure 3m

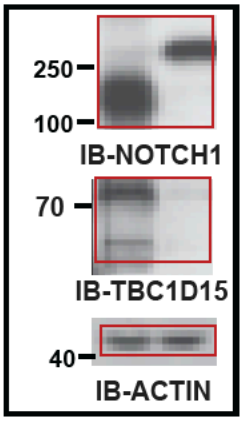

Figure 3p

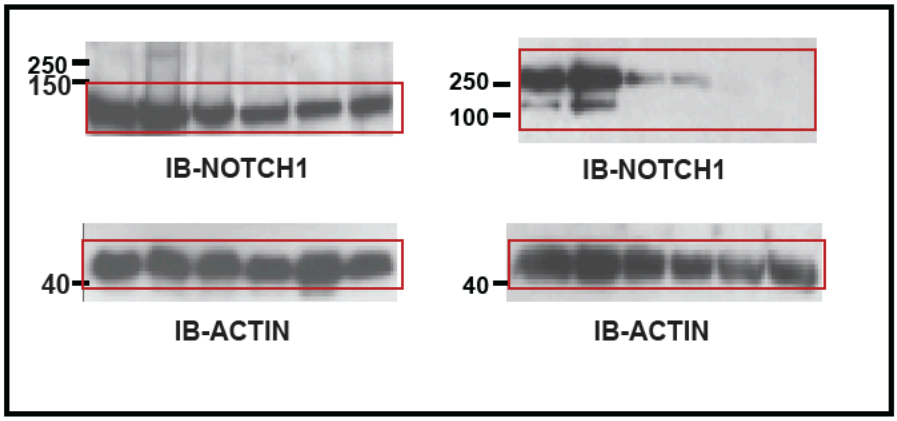

Figure 4b

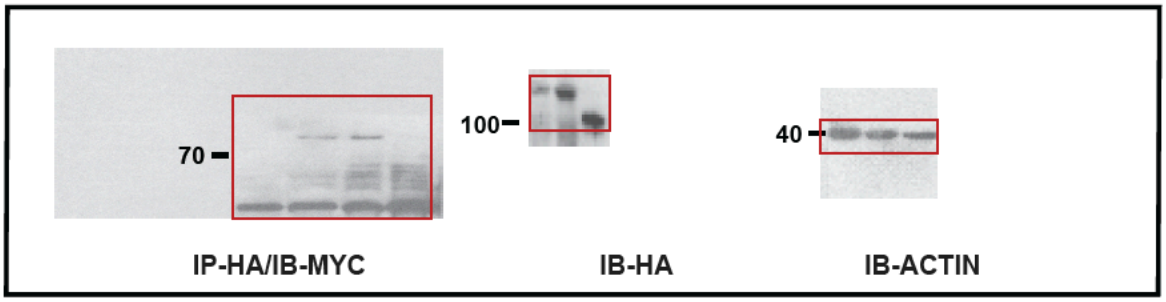

Figure 4c

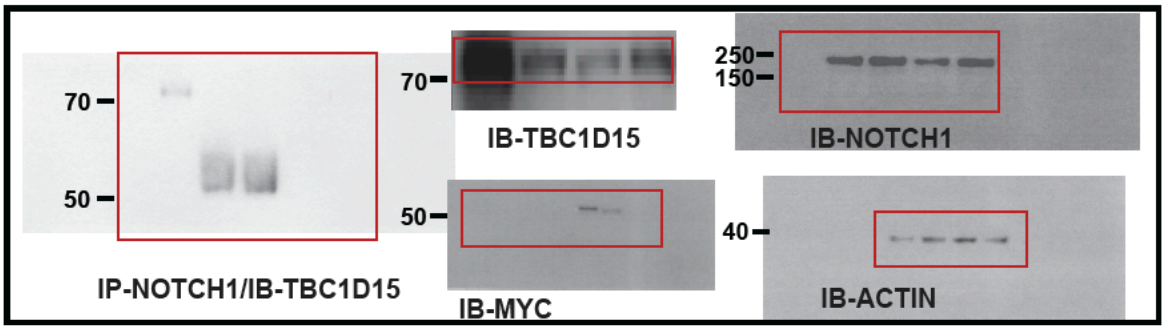

Figure 4d

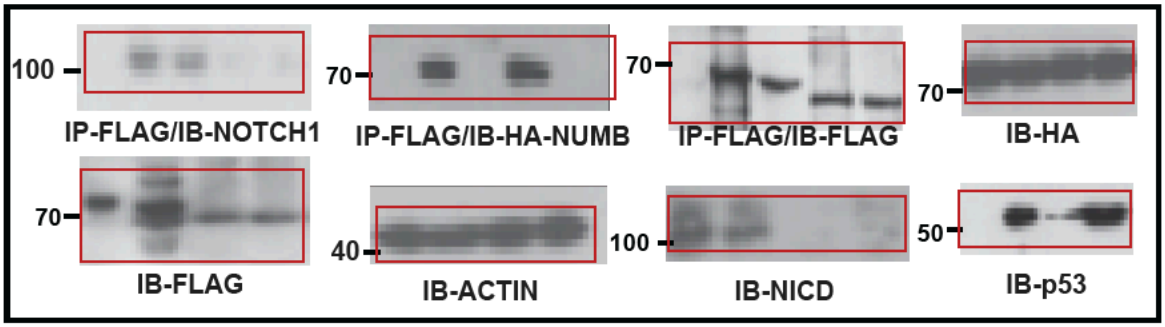

Figure 5a

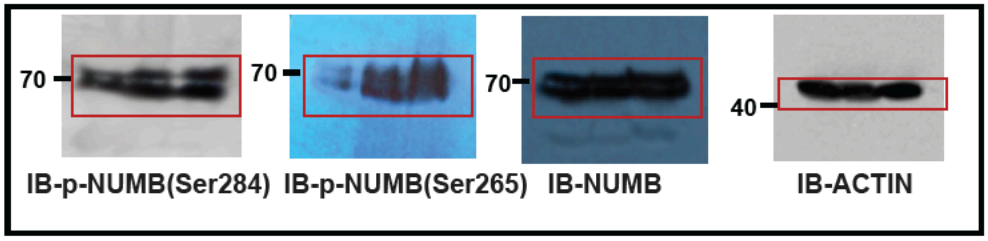

Figure 5b

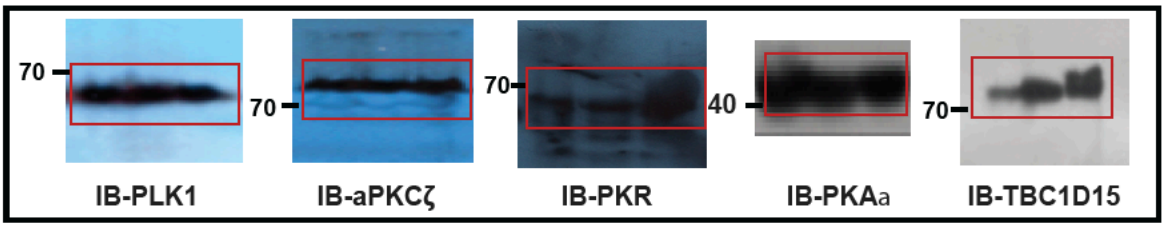

Figure 5e

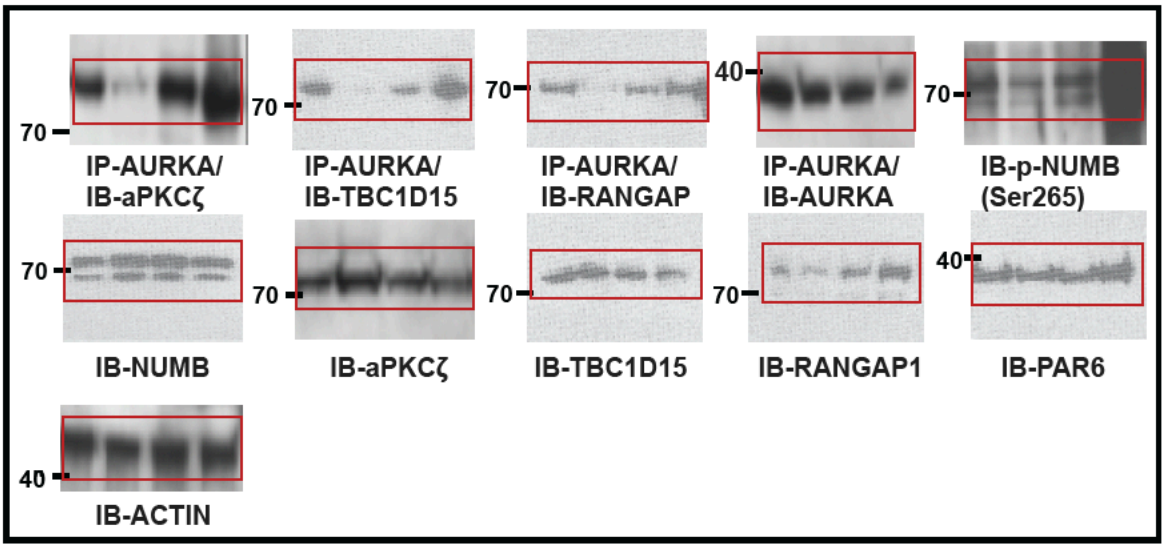

Figure 5f

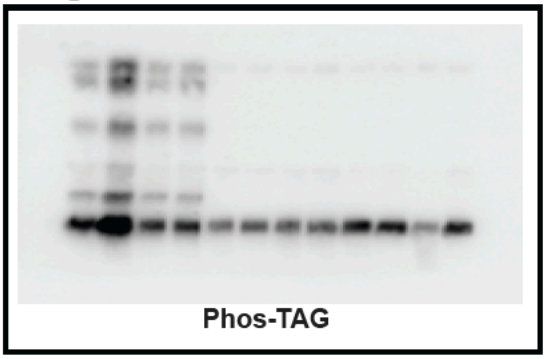

Figure 6e

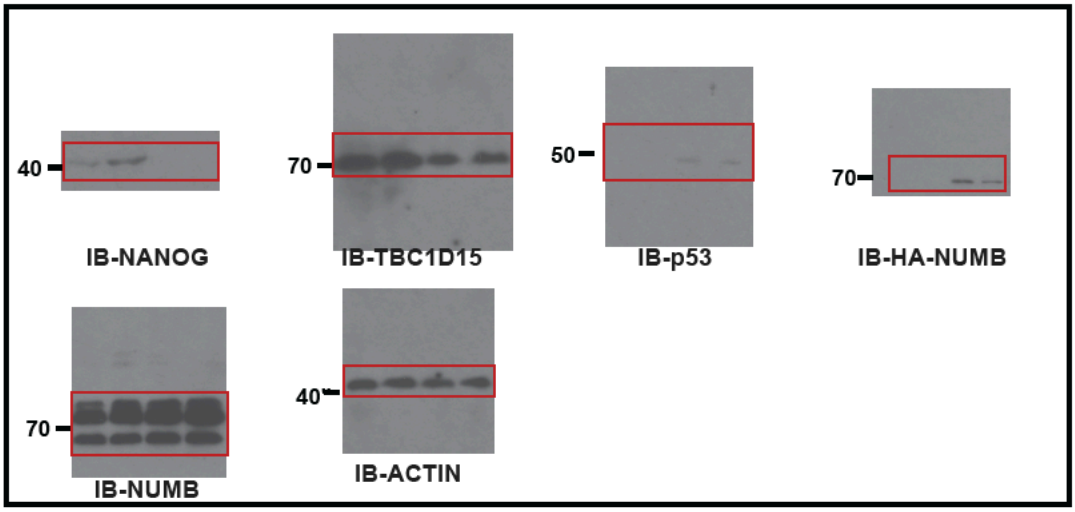

Figure 6h

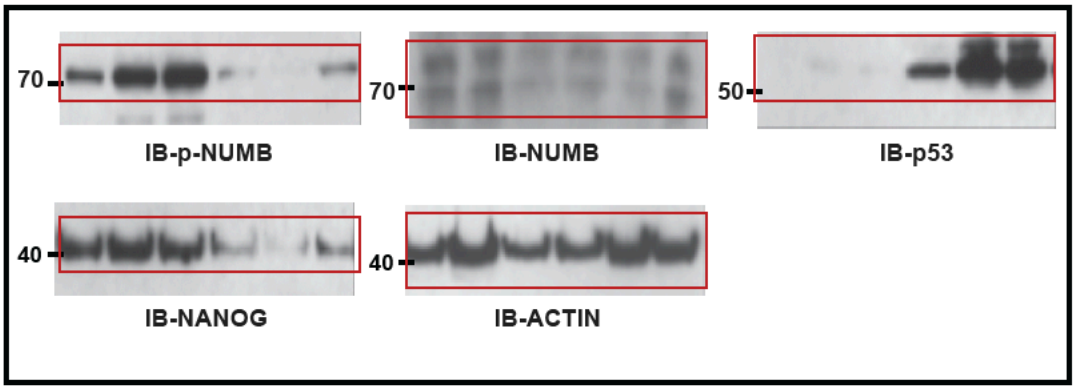

Supplementary Figure 10. Gating for FACS analyses.

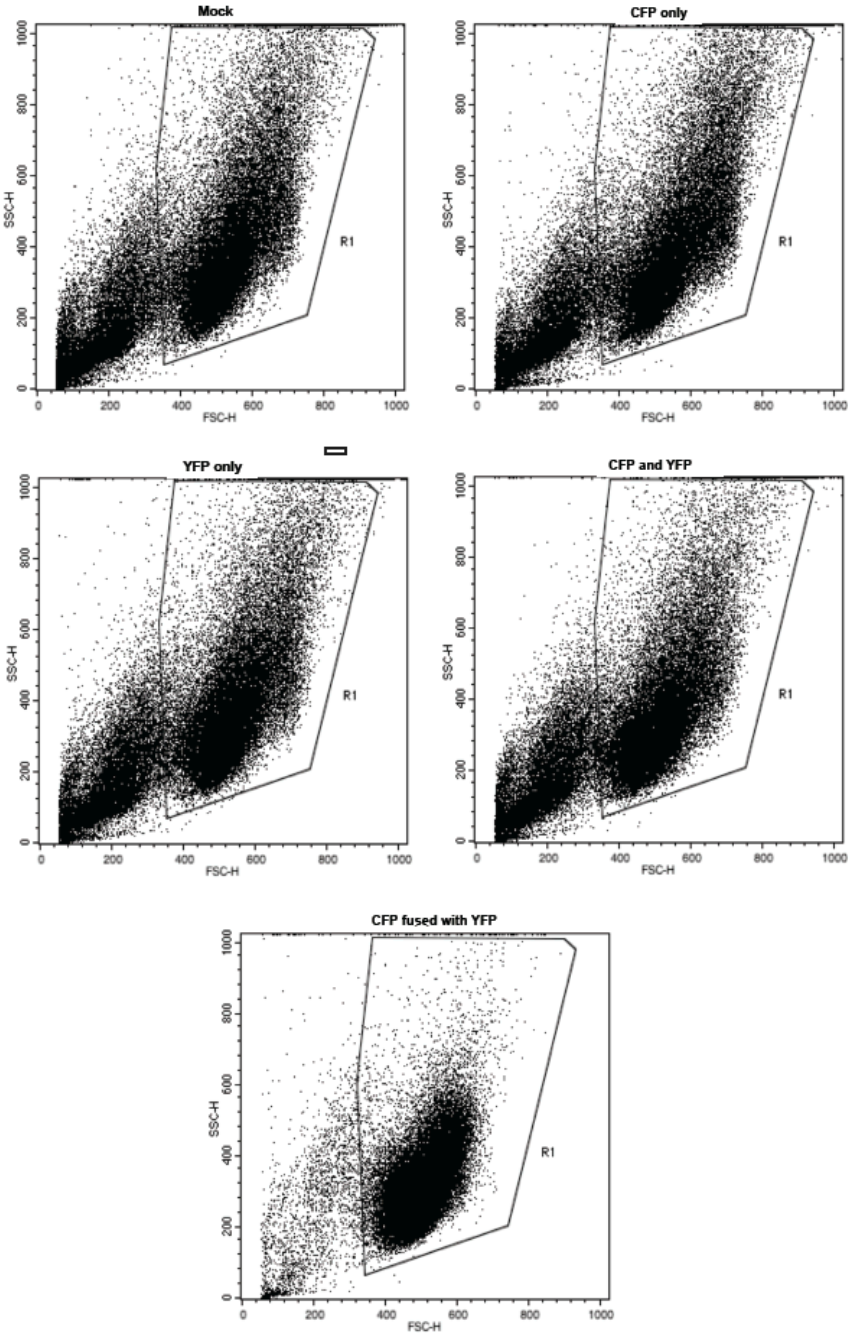

Supplementary Fig. 10
Choi and Siddique et al.

- **CONTACT FOR REAGENT AND RESOURCE SHARING**

Further information and requests for resources and reagents should be directed to and will be fulfilled by the Lead Contact, Keigo Machida (Keigo.machida@med.usc.edu).

Supplementary Methods

- **Genetically manipulated mouse models:** We generated a conditional *Tbc1d15* knockout mouse model with the help of the International Knockout Mouse Consortium. All the background transgenic mice were created and bred by us. *Cre-ERT2* Tg mice (obtained from Drs. Daniel Metzger and Pierre Chambon, IGBM, Illkirch, France: **Fig. 1d**) allowed tamoxifen activation of *Cre* for removal of a floxed stop sequence for specific gene expression induction. To determine the causal roles of NUMB phosphorylation and TBC1D15 oncoprotein in alcohol-induced liver tumorigenesis in HCV-Tg mice, we generated *Alb::CreERT2*:*non-phosphorylatable mutant Numb-3ALSL* mice (Conditional expression of *Numb-3A* in ROSA26 locus downstream of a floxed stop sequence: *Lox-Stop-Lox*, *LSL*) and cross-bred these with *Ns5aTg* mice to produce *Numb-3ALSL:Ns5aTg* and *Alb::CreERT2:Numb-3ALSL:Ns5aTg* mice under the congenic background. The knock-in approach of three non-phosphorylatable amino cid substitutions is ideal, but was a challenging task since the three phospho-serines (S7, S265, S284) of wt NUMB region in a 134 kbp-genomic region. Male *Ns5aTg* mice fed a modified Lieber-DeCarli (L-D) alcohol diet had a 32% liver tumor incidence (female mice exhibited a lower incidence rate of 18%)[7]. To initiate overexpression of NUMB-3A, mice were injected intraperitoneally five times with tamoxifen at two-day intervals before the initiation of L-D diet feeding at the age of two months of age. Tamoxifen injection may affect alcohol-induced liver damage, and consequently, liver tumorigenesis in these models, as estrogen is known to aggravate alcoholic liver disease in mice [41, 42]. To exclude artifact from repetitive tamoxifen injection, the control group was also treated with tamoxifen. After feeding for nine months, mice were examined monthly for tumors by abdominal ultrasound using the VisualSonics' Vevo 770 High-Resolution Imaging System (at the Molecular Imaging Center of USC). This allowed the 3D visualization and volume measurements of liver tumor masses.
- *Tbc1d15*$^{Flox/Flox}$ mice were generated such that the genomic region containing exons 4, 5, and 6 of Tbc1d15 gene, encoding most of the NUMB-binding domain (aa 69-229 aa) was floxed by stuffer sequence (STOP codon). These mice were crossed with *Alb::CreERT2* and *Ns5aTg* mice to generate the compound mice in the congenic C57Bl/6 background. To determine the effects of TBC1D15 deficiency on liver tumor latency, incidence, and size*, Alb::CreERT2; Tbc1d15*$^{Flox/Flox}$*;Ns5aTg* and *Tbc1d15*$^{Flox/Flox}$*; Ns5aTg* mice were injected with tamoxifen (i.p.) and fed alcohol/WD for 12 months.
- **Sample preparation for LC/MS-MS:** The denatured samples were, reductively alkylated with iodacetamide, and trypsin-digested with trypsin as described previously[43].
- **TCGA data analyses:** We performed meta-analysis of public datasets (TCGA, GSE17856, GSE27150) of liver cancer patients. We correlated gene expression with matched clinical data. A subset of these data had gene expression information corresponding to various stages of liver cancer including metastasis was generated. The patient data were divided into early stages of tumor progression for correlation with the expression of Notch1 and TBC1D15 during tumor progression. A t-test was performed to estimate the differences in expression of Notch1 and TBC1D15 genes in early and late metastatic stage of liver cancer patients.
- **aPKCζ pseudosubstrate inhibitor (PPI):** One hour after drug challenge (five times a week for four weeks of treatment) on days 28, intratracheal instillation with 10μg/mouse of aPKCζ pseudosubstrate attached to cell permeabilization vector peptide (Tocris, Minneapolis, MO, USA)[44] into the tumor-beraing mice (10μg/mouse) was performed non-operatively. Inhibitor of

atypical protein kinase C (aPKC) ζ is attached to cell permeabilisation Antennapedia domain vector peptide.

- ***In vitro* kinase assays:** Aurora A and aPKCζ were measured by SignalChem Kinase activity assay Kits as described previously[12].
- ***In vivo* mouse imaging:** Each month following prior nine months of alcohol-Western diet, mice were examined for tumors by abdominal ultrasound using the VisualSonics' Vevo 770 High-Resolution Imaging System (Molecular Imaging Center at USC) which allows the 3D visualization and volume measurements of the liver tumor masses. Tumor burden was monitored monthly by measuring the body weight, which according to IACUC guidelines cannot exceed more than 5% of the control body weight.
- **IP-western blots:** We obtained NOTCH truncation mutants (Full-length, ΔΔ-E, TM-RAM, RAM , and NICD) from Dr. Chengyu Liang (USC) for the purpose of domain-mapping of NOTCH for its interaction with TBC1D15 protein. We transfected human NOTCH1 constructs together with a TBC1D15 construct to determine domains of NOTCH1 that interacts with TBC1D15. We performed IP-Western analyses to examine the solution interaction between TBC1D15 and NOTCH1. NOTCH1 C-20 antibody (1:1000 dilution for Western blot analyses: SIGMA) was used for these analyses.
- **Immuno-affinity purification and tandem Mass-spectrometry:** We used on-line LC-Orbitrap XL CID MS/MS instrument to identify a potential interacting protein with TBC15. We did trypsin digestion of IP samples separated by SDS-PAGE. Gel pieces were then subjected to a modified in-gel trypsin digestion procedure[36].
- **Simulation of docking between TBC1D and NuMA1 or NOTCH1:** Based on the domain section of NUMA, NUMA aa 1788 to the end portion was simulated into the structure. The TBC1D15 of this structure is used to dock with NUMA from 3ro2 with LGN. The interacting residues from NUMA to LGN are: ('2', 'GOL'), ('3', 'GOL'), ('7', 'HOH'), ('11', 'HOH'), ('18', 'LEU'), ('21', 'ALA'), ('22', 'LEU'), ('25', 'GLU'), ('28', 'CYS'), ('29', 'LYS'), ('40', 'PHE'), ('52', 'LYS'), ('53', 'THR'), ('55', 'SER'), ('56', 'ALA'), ('59', 'SER'), ('60', 'GLN'), ('63', 'ASN'), ('64', 'ALA'), ('66', 'PHE'), ('81', 'ASP'), ('85', 'ALA'), ('93', 'GLY'), ('96', 'LYS'), ('103', 'ASN'), ('106', 'LYS'), ('107', 'VAL'), ('136', 'ARG'), ('139', 'TYR'), ('140', 'ASN'), ('143', 'ASN'), ('146', 'HIS'), ('150', 'LYS'), ('196', 'ARG'), ('199', 'GLY'), ('200', 'ASN'), ('203', 'ASN'), ('206', 'TYR'), ('207', 'LEU'), ('221', 'ARG'), ('235', 'ARG'), ('236', 'ARG'), ('240', 'ASN'), ('243', 'ASN'), ('246', 'ILE'), ('247', 'PHE'), ('276', 'GLN'), ('279', 'TYR'), ('280', 'SER'), ('283', 'ASN'), ('316', 'ARG').

  Analyses of 3D structure of TBC1D15-NOTCH1 interaction identified TBC1D15 N terminal region (green) docking with _a.a.1805-2113 of NOTCH1 (blue). Inhibitor A efficiently binds both interactions domains for TBC1D15-NOTCH and TBC1D15-NUMB. Interface residues from TBC1D15 (red) are: ('17', 'GLY'), ('19', 'TYR'), ('139', 'LYS'), ('140', 'GLN'), ('141', 'ASN'), ('142', 'LYS'), ('143', 'GLU'), ('144', 'GLY'), ('145', 'MET'), ('146', 'GLY'), ('147', 'TRP'), ('165', 'PHE'), ('166', 'HIS'), ('167', 'GLN'), ('168','GLY') and ('171','LYS'). Inhibitor A: (5Z,9α,11α,15R)-9,11,15-Trihydroxy-17-phenyl-18,19,20-trinor-prost-5-en-1-oic acid.
- **Statistical Considerations:** For this study, HCC from three etiological backgrounds were used for PDX models: HCC can be attributed to ALD and NASH as these metabolic liver diseases are increasingly associated with HCC incidence. HCC from HCV or HBV patients were not included in this study because different viral genotypes may exhibit confounding different phenotypes and HCV- or HBV-infected PDX models pose a significant logistical challenges from the biosafety standpoint.
- **NCBI tracking system number:**
  - The data used in this study has been deposited to NCBI under **GSE61435 (Microarray)** and **GSE68237 (ChIP-Seq)**.
  - Human Gene expression profiling by array[40]: **GSE17856** and **GSE27150**

- **EXPERIMENTAL MODEL AND SUBJECT DETAILS**
  - In vivo animal studies

- **Genetically manipulated mouse models**
- We generated a conditional Tbc1d15 knockout mouse model with the help of the International Knockout Mouse Consortium. All the background transgenic mice were created and bred by us. Cre activation mediated removal of a floxed stop sequence upon tamoxifen induction of Cre-ERT2 Tg mice (obtained from Drs. Daniel Metzger and Pierre Chambon, IGBM, Illkirch, France: **Fig. 1d**). To determine the causal roles of NUMB phosphorylation and TBC1D15 oncoprotein in alcohol-induced liver tumorigenesis in HCV-Tg mice, we generated *Alb::CreERT2*:*non-phosphorylatable mutant Numb-3ALSL* mice (Conditional expression of *Numb-3A* in ROSA26 locus downstream of a floxed stop sequence: *Lox-Stop-Lox*, *LSL*) and crossed with *Ns5aTg* mice to produce *Numb-3ALSL:Ns5aTg* and *Alb::CreERT2:Numb-3ALSL:Ns5aTg* mice under the congenic background. Knock-in approach of three non-phosphorylatable mutations is ideal, but was a challenging task since the three phospho-serines in the wt gene reside (S7, S265, S284) in a 134 kbp-genomic region. Male *Ns5aTg* mice fed a modified Lieber-DeCarli (L-D) alcohol diet had a 32% liver tumor incidence (female mice had a lower incidence rate of 18%)[7]. To initiate overexpression of NUMB-3A, mice were injected intraperitoneally five times with tamoxifen at two-day intervals before the initiation of feeding at the age of two months of age. Tamoxifen injection may affect alcohol-induced liver damage, and consequently, liver tumorigenesis in the models as estrogen is known to aggravate alcoholic liver disease in mice[41]. To exclude artifact from repetitive tamoxifen injection, the control group was also injected with tamoxifen. Each month after feeding for nine months, mice were examined for tumors by abdominal ultrasound using the VisualSonics' Vevo 770 High-Resolution Imaging System which allows the 3D visualization and volume measurement for liver tumor mass at the Molecular Imaging Center at USC.
- *Tbc1d15*$^{Flox/Flox}$ mice were generated in which a genomic region containing exons 4, 5, and 6 of the gene, encoding most of NUMB-binding domain (69-229 aa) that promotes p53 degradation, is floxed by stuffer sequence (STOP codon). These mice were crossed with *Alb::CreERT2* and *Ns5aTg* mice to generate the compound mice in the congenic C57Bl/6 background. To determine the effects of TBC1D15 deficiency on liver tumor latency, incidence, and size*, Alb::CreERT2; Tbc1d15*$^{Flox/Flox}$*;Ns5aTg* and *Tbc1d15*$^{Flox/Flox}$*; Ns5aTg* mice were injected with tamoxifen (i.p.) and fed alcohol/WD for 12 months. Sibling controls and alcohol-WD was fed the identical diet but with dextrin replacing alcohol. After nine months of feeding, mice were examined monthly for tumors by abdominal ultrasound using the VisualSonics' Vevo 770 High-Resolution Imaging System as described above. At the terminal point, liver tumor incidence, size, and weight were recorded. Liver biochemistry and immunostaining were performed for the key parameters of aPKC-NUMB-p53 and TBC1D15 pathways as already described above for the NUMB-3A overexpression model.
- Each month after feeding for nine months, mice were examined for tumors by abdominal ultrasound using the VisualSonics' Vevo 770 High-Resolution Imaging System which allows both 3D visualization and volume measurement of liver tumor mass. Tumor burden was monitored monthly by measuring the body weight, which according to USC IACUC guidelines was not exceed more than 5% of the control body weight.

- **METHOD DETAILS**

Immuno-affinity purification and tandem Mass-spectrometry

We used LC-Orbitrap XL CID MS/MS to identify a potential interacting protein with TBC1D15. We did in-gel digestion of IP samples separated by SDS-PAGE. Gel pieces were then subjected to a modified in-gel trypsin digestion procedure[36]. Peptides were collected and subjected to LC-MS/MS sequencing and data analysis. The identification of TBC1D15 and its interacting proteins were carried out by mass spectrometry and validated by another functional assay. By using of strict scoring metrics, we identified several high-confidence interacting proteins, including

NOTCH1, 2, 3, and 4, NuMA1, and RanGap1. RANGAP1 is a crucial regulator of RAN-GTP/GDP cycles and mitosis coordinator and known to regulate expression of AURKA[20].

PRIDE Submission Reference Number: 1-20200414-55525

LC/MS/MS Analysis

For LC/MS-MS, the sample was denatured, reduced with DTT, alkylated with Iodacetamide, and digested with trypsin as described previously. Protein sequences were analyzed by use of an LC/MS system with LTQ Orbitrap XL (Thermo Fisher Scientific, San Jose, CA) and an Eksigent NanoLC Ultra 2D (Dublin, CA) as previously described[36]. Peptides were separated with 5 µm C18 beads packed in a 10 cm column (75 µm inner diameter) on a Eksigent NanoLC Ultra 2D system by use of a binary gradient of buffer A (0.1 % formic acid) and buffer B (80% ACN and 0.1% formic acid). The peptides were loaded with buffer A (at a flow rate of 300 nL/min). Peptides were eluted with a linear gradient from 10% to 35% buffer B in 95 min followed by 50% B for 15 min (at a flow rate of 250 nL/min). The column was washed with 90% buffer B and equilibrated with 5% buffer B for 10 min. The eluates were sprayed into the LTQ Orbitrap XL with the ion transfer tube at 250 °C at 2.1-2.25 kV with no sheath gas flow. After accumulation to an AGC target value of 500,000 in the linear ion trap with 1 microscan, MS spectra were obtained in the orbitrap in the range of m/z 350–2,000 at a FWHM resolution of 30,000.

The precursors selected for fragmentation by collision-induced dissociation (CID) were processed for peptide sequencing and modification site localization. Fragment ions were examined in the liner ion trap. The five most abundant precursor ions were chosen for fragmentation by CID. The data-dependent acquisition mode was selected while five CID data-dependent MS/MS scans came after the high-resolution MS scan. For all sequencing events, dynamic exclusion was enabled to minimize repeated sequencing. Peaks selected for fragmentation more than once within 60 s were excluded from selection (10 ppm window).

Data Processing of LC/MS/MS

Proteome Discoverer 1.4 (Thermo Fisher Scientific) was used for protein identification using Sequest algorithms. The following criteria were followed. For MS/MS spectra, variable modifications were selected to include M oxidation and C carbamidomethylation with a maximum of four modifications. Searches were conducted against Uniprot or in-house customer database. Up to two missed cleavages were allowed for the proteolytic enzyme and protease digestion. Peptides were fully tryptic. MS1 tolerance was 10 ppm. MS2 tolerance was set at 0.8 Da. If peptides met the false discovery rate of 1%, peptides reported were accepted via search engine. No fixed cutoff score threshold was in place while until the 1% FDR rate is reache, spectra were accepted. Peptides with a minimum of six amino acid lengths were processed for identification. the mass spectra were mannually inspected and validated.

TCGA data analyses

From public datasets (TCGA, GSE17856) of liver cancer patients showing gene expression and matched clinical data, a subset of data showing gene expression corresponding to various stages of liver cancer including metastasis was generated. A representative Box plot showing the expression of Notch1 and TBC1D15 in non-tumor normal (n= 62) early stage of cancer (n= 284) and late (n=102) metastatic stages of liver cancer patients. The samples were divided into early stage and late metastatic stage of tumor progression to correlate the expression of Notch1 and TBC1D15 in tumor progression. The early stage non-metastatic samples showed an average combined expression of both genes as 8.8 (range of 0.1-12), while late stage metastatic samples with an average of 14.7 (range 13- 18). The box whisker plot representing interquartile range (IQR) of minimum, 25th percentile, median, 75th percentile and maximum values show that more aggressive tumors have a higher combined expression of Notch1 and TBC1D15. A t-test was performed to estimate the differences in the expression of Notch1 and TBC1D15 genes in early and late metastatic stage of liver cancer patients as well as normal non tumor individuals.

Animal Treatment

These mice were fed modified high-fat Lieber-DeCarli (L-D) liquid diet (Bioserv, NJ) with alcohol (3.5%w/v) and high-fat or isocaloric dextrin using glass tubings for 3 months from 2 months of age (every day the diet is renewed). Based on the predicted incidence rates of HCC and attrition rates (15-30%) in the different genetic and dietary groups and the power analysis using the 80% power and a p-value of 0.05, the numbers of mice required for statistical analysis of the outcome in this study are derived. This formula of alcohol liquid diet has been used for many research institutions in worldwide (Lieber-DeCarli diet) and our previous study shows that the calorie intake between alcohol diet and control diet is not statistically different.

aPKCζ pseudosubstrate inhibitor (PPI)

One hour after a challenge (five times a week for four week-treatment) on days 28, intratracheal instillation with 10μg/mouse of aPKC ζ pseudosubstrate attached to cell permeabilization vector peptide (Tocris, Minneapolis, MO, USA)[44] into the tumor-beraing mice (10μg/mouse) was performed non-operatively. Inhibitor of atypical protein kinase C (aPKC) ζ is attached to cell permeabilisation Antennapedia domain vector peptide. Consists of amino acids 113-129 of aPKC ζ pseudo substrate domain linked by a disulfide bridge to the Antennapedia domain vector peptide. The Antennapedia peptide is actively taken up by intact cells, at 4 or 37°C, ensuring rapid and effective uptake of the inhibitor peptide. Once inside the cell, the disulfide bonds are subjected to reduction in the cytoplasm leading to the release of the inhibitor peptide. Induces mast cell degranulation by a PKC ζ-independent pathway.

Sequence: CRQIKIWFQNRRMKWKK CSIYRRGARRWRKLYRAN* (Modifications: Disulfide bridge between 1 -1*) and RLYRKRIWRSAGR sequences (ZIP) were used as scrambled (http://www.tocris.com/dispprod.php?ItemId=212092#.VQNbXOG2L2c,

Effect of intrathecal administration of ZIP on mechanical and thermal sensitivity or locomotor function in normal rats Intrathecal scrambled peptide (10 μg, n=8) did not modify mechanical and thermal withdrawal responses compared to baseline in normal mice. More interestingly, intrathecal administration of 10μg (n = 8) of ZIP did not alter mechanical and thermal withdrawal responses compared to baseline, and the control scrambled peptide group throughout the whole experiment. Finally, neither the control scrambled peptide nor ZIP had any effect on the loco-motor function of rats on the rotarod, assessed at 30 and 60 min post-injection.

***In vitro* kinase assays**

Aurora A and aPKCζ were measured by SignalChem Kinase activity assay Kits as described previously. Briefly, after immuno-precipitation, samples were incubated in 20 μl reaction mixture containing each substrates and buffers. Next, 5 μl of γ-[^{32}P] ATP assay cocktail was added, the mixture was incubated in a water bath at 30^{o}C for 15 min. Then, 20 μl of the reaction mixture was spotted onto individual pre-cut strips of of phosphocellulose p81 paper (Millipore, Temecula, CA), and the dried strips were washed three times with 1.0% phosphoric acid solution. Radioactivity on the p81 paper was scored in presence of scintillation fluid on a liquid scintillation analyzer (Packard Instrument Co.). The activities were presented in the figure as γ-[^{32}P] ATP specific activity or Kinase specific activity. To test if TBC1D15-mediated positive regulation of aPKCζ activity, we directly tested whether TBC1D15 increases NUMB phosphorylation in a manner dependent on aPKCζ or/and AURKA by using Huh7 cells transduced with Flag-NUMB, aPKCζ, AURKA, and/or TBC1D15 and incubated with γ-[^{32}P] ATP. Following cell lysis, Flag-NUMB was immunoprecipitated and immunoblotted for autoradiography. We also treated the cells with the AURKA inhibitor MK5108 to test the contribution of this kinase. Flag-NUMB phosphorylation modestly increased with the expression of aPKCζ and AURKA but conspicuously increased with the concomitant expression of TBC1D15 and this effect was attenuated in the absence of AURKA and dose-dependently abrogated by the AURKA inhibitor MK5108. These results collectively suggest TBC1D15 positively upregulates AURKA activity and NUMB phosphorylation to drive symmetric division.

NUMB Phosphorylation Analyses

The effects on NUMB phosphorylation were assessed by incubating the cells with ^{32}P-orthophosphate in phosphate-free DMEM with 10% dialyzed FBS for 4 hours, followed cell lysis, NUMB immunoprecipitation, PAGE, and autoradiography to monitor incorporation of ^{32}P into NUMB[12, 37]. p53 dissociation from NUMB and p53 levels were assessed by co-IP and IB. Self-renewal activity was evaluated through methylcellulose spheroid formation assays and Colony formation assay as previously described[38].

***In vivo* mouse imaging**

Each month after feeding for nine months, mice were examined for tumors by abdominal ultrasound using the VisualSonics' Vevo 770 High-Resolution Imaging System which allows the 3D visualization and volume measurement for liver tumor mass at the Molecular Imaging Center at USC. Contrast-enhanced micro-CT and texture-based volume renderings (VRT) were performed to demonstrate a reduction of tumor size and to measure tumor volume based on 3D data collected using Inveon CT (Siemens Medical Solutions, Knoxville, TN) at a voxel size of (10^6 μm^3). Tumor burden was monitored monthly by measuring the body weight, which according to IACUC guidelines cannot exceed more than 5% of the control body weight.

FRET assays

Live cells were gated according to forward and sideward scatter (FSC/SSC) and photomultiplier tube (PMT) voltages was adjusted, and FRET was evaluated in double positive cells as compensation for CFP and YFP. When excited at 405 nm, YFP showed some emission in the FRET-channel. As YFP is excited at 405 nm (FRET/YFP), an additional gate was introduced to exclude cells exhibiting false-positive signals from FRET channel. A triangular gate was introduced to FRET versus CFP was plotted and the amounts of FRET-positive cells were examined (**Fig. 2h, bottom**). The triangular gate was adjusted to measure cells transfected with CFP and YFP[34, 35].

Immunoprecipitation-Western Blot

We obtained NOTCH truncation mutants (Full-length, ∆-E, TM-RAM, RAM , and NICD) from Dr. Liang's lab to do domain-mapping of NOTCH to interact with a trafficking protein TBC1D15. We transfected hNOTCH1 constructs with a TBC1D15 construct to see if which domain of NOTCH1 interacts with TBC1D15. We performed IP-Western analyses to examine the interaction between TBC1D15 and NOTCH1. NOTCH1 C-20 antibody (1:1000 dilution for Western blot analyses: SIGMA) was used.

In detail, Huh7 (differentiated hepatocyte-derived carcinoma cell line) were cultured in DMEM high glucose media supplemented with 10% FBS and 0.1% non-essential amino acids in T25 flask and were co-transfected with NOTCH1 full-length constructs together with TBC1D15 truncation mutants in one group and TBC1D15 Full-length construct together with NOTCH1 truncation mutants in the other group. The TBC1D15 truncation mutants that were used were: Full Length mTBC1D15-FLAG, mTBC1D15 N-Terminus-FLAG, mTBC1D15-F1-2KR-FLAG, MTBC1D15-CΔC-FLAG, shTBC1D15-685 and shTBC1D15-963. NOTCH1 constructs that were used were: hNOTCH1-Full-length-myc, hNOTCH1 ΔE-3myc, hNOTCH1 TMRM-3myc, hNOTCH1ΔEΔDRAM-3myc, mNOTCH1 ΔEΔPEST-myc and hNOTCH1 ΔE V1754L. BioT was used as the transfection reagent (Bioland Scientific LLC, B01-01). Cells were lysed with Triple detergent lysis buffer after 48 hours post-transfection, and half of the lysates were used for total lysate analysis while the other half were used for immunoprecipitation (IP). IP lysates were pre-cleared for one hour with 20μL protein A/G beads (Santa Cruz Biotechnologies, sc-2003) and incubated overnight in 4°C with anti-flag tag (Thermo Fisher Scientific, MA1-91878) or anti-Myc tag antibody (EMD Millipore Corp, 05-274) on a rotation device. In the next day, protein A/G beads were pulled down and washed with triple detergent lysis buffer and boiled in 6 × loading dye followed by electrophoresis by SDS-PAGE and protein analysis by nitrocellulose membrane.

Huh7 cells were transfected with TBC1D15 full-length construct by Bio-T. The media was replaced 24 hours after transfection. The cells were lysed with Triple detergent lysis buffer at 48

hours post-transfection. IP lysates were incubated for 2 hours in 4°C with 1.0 µg of the appropriate control IgG (corresponding to the host species of the NuMA1 antibody, Santacruz biotechnology, SC-2025) and NuMA1 antibody (BD Biosciences, 810561) on a rotation device. After two hours, these lysates were added protein A/G beads (20 µl of 50% bead slurry) and incubated with gentle rocking for one hour 4°C. Immunoprecipitates were washed with triple detergent lysis buffer and resuspended/boiled in the immunoprecipitate pellets with 10 µl 6 × Laemmli sample buffer for 5 min.

Purification of Recombinant Proteins

To purify flag-TBC1D15, and GFP-NuMA1 wild type/mutants (T1804A, S2047A T1991A) proteins, HEK-293A cells were grown to 70–80% confluence and transfected with 10 µg plasmid constructs [flag-TBC1D15, and GFP-NuMA1 wild type/mutants (T1804A, S2047A T1991A)], individually. Cells were washed once with cold PBS 48 hours post-transfection, and lysed with 1 ml cold NP-40 Lysis Buffer (10 mM HEPES pH 7.5, 10 mM KCl, 1.5 mM MgCl2, 0.5% NP-40) for one hour on ice, followed by centrifugation at 13,000 x g for 10 min and collection of the supernatant. For each immunoprecipitation, 1 mg supernatants were incubated with 30 ml of a 40% slurry of M2 anti-Flag agarose or with 1 µg anti-GFP antibody for 2 hours at 4°C with rotating. The reaction mixture 30 µl of a 25% slurry of protein G-agarose was added, and all samples were incubated for an additional 2 hours. Agarose-beads were washed once in Buffer W (20 mM Tris pH 7.3, 300 mM NaCl, 0.5% triton X-100, 2% glycerol), washed once with PBS containing 0.2% Triton X-100, and washed once with PBS. Flag-TBC1D15 were eluted by incubation with 3 x Flag peptide (1 mg/mL, Invitrogen) overnight at 4°C with rotating. All samples were stored at -80°C in PBS containing 5% glycerol and 1 mM DTT.

***In vitro* Protein Interaction Assays**

For purified recombinant Flag-TBC1D15, we were incubated with GFP-NuMA1 (wild type and mutants)-conjugated agarose resin for 45 min at room temperature with rotating. Samples were washed twice with Buffer W and washed once with cold PBS. Then, it was boiled in 6 x Laemmle sample buffer prior to analysis by SDS-PAGE.

***In vitro* Kinase Assays**

Kinase assays were carried out using 2 ng of the purified kinase domain of Aurora-A (Millipore Ltd, 14-511) incubated with 10 µg of the Flag-TBC1D15 and GFP-NuMA1 (wild type and mutants). The reagents were incubated for 30 minutes at 30° C in kinase buffer consisting of 20 mM HEPES pH 7.5, 5 mM $MgCl_2$, 0.2 M KCl, 0.5 mM EGTA, 2 mM DTT, 0.25 mM $NaVO_4$, and 1 mM ATP. For the phosphorylation time-course, kinase reactions were stopped by addition of 6 x Laemmli sample buffer. To differentiate the phospho-proteins from their non phosphorylated counterparts, samples were separated by Phos-TAG SDS- PAGE (Wako Pure Chemical Industries, Ltd, AAL-107).

Human tissue specimens

The paraffin-embedded tissue sections of human hepatocellular carcinoma (HCC) were obtained from the University of Minnesota Liver Tissue Cell Distribution System. All tissue sections were obtained from patients with informed consent prior to surgery, in accordance with the approved protocol of the Institutional Review Board of the University of Minnesota, Minneapolis. The tissue sections were obtained from de-identified patients (43-67 years old) with alcohol and/or viral hepatitis associated liver tumors of varying grades. Non-tumor tissues were obtained from clearly delineated margins of surgical specimens.

Immunostaining

Tissue sections were re-hydrated by immersion in xylene (3 × 5 mins) followed by continued re-hydration steps in 100%, 90% and 70% ethanol. Following washing in PBS (3 × 5 min), antigen retrieval was performed in 10mM sodium citrate (pH 6.0) at 90 °C for 1 hour and slides were then allowed to cool down to room temperature. Following antigen retrieval, tissues were blocked in

5% goat-serum and 0.3% TritonX in BSA for overnight in 4C with primary antibody for TBC1D15 and NOTCH1 (1:1) at 1:100 ratio. Fluro-conjugated secondary antibody (Invitrogen) was added the next day at a 1:100 ratio and DAPI containing mounting media was then used to complete the staining process. Slides were then imaged using a Leica Fluorescence microscope on the SP8 software.

Dual Luciferase Assay

Huh7 cells were treated either with shTBC1D15 lentivirus or with sh-Scrambled lentivirus in T25 flask. After 48 hours, the cells were spit into 6-well plates. Following a 24-incubation period, the cells were treated with Hey1 and Hey2 promoter constructs using BioT as the transfection reagent and transfection was done in triplicates. Constructs used were: pluc Hey1, pluc Hey1 Δ215, pluc ΔSac I/Hind III, plucΔ41, PGI3-Hey2, RPBJ-mutB and pGL-BASIC. 48 hours following transfection, the cells were washed in cold PBS and then lysed using passive lysis buffer. After lysis of the cells, the cell lysates were added to LARII reagent and then measurements were taken for firefly lucifrase activity. Stop and Glo was added to stop the reaction and measurement was then taken for the *Renilla* Luciferase activity to obtain a *Firefly* to *Renilla* ratio.

NOTCH1 stability

Huh7 cells were transduced with scrambled shRNA (sh-Scr) or shRNA targeting TBC1D15. Two days after transfection, culture medium was replaced by methionine-free medium and the cells were labeled with ^{35}S- methionine for 60 min. Cycloheximide (CHX) was added and cells were harvested at the indicated times afterwards.

Immuno-affinity purification and tandem Mass-spectrometry

We used on-line LC-Orbitrap XL CID MS/MS to identify a potential interacting protein with TBC15. We did in-gel digestion of IP samples separated by SDS-PAGE. Gel pieces were then subjected to a modified in-gel trypsin digestion procedure[36]. Peptides were collected and subjected to LC-MS/MS sequencing and data analysis. The identification of TBC15 and its interacting proteins were carried out by mass spectrometry and validated by another functional assay. By using strict scoring metrics, we have identified several high-confidence interacting proteins, including NuMA1, and RanGap1. RANGAP1 is a crucial regulator of RAN-GTP/GDP cycles and mitosis coordinator and known to regulate expression of AURKA[20].

Pathological analysis

At the end of 12 months, the mice were euthanized and liver tumors measured, weighted, and collected for histological (H&E), biochemical (IB for TLR4, NANOG, p-NUMB, NUMB, p53, TBC1D15), and immunohistochemical (NANOG, p-NUMB, p53) analyses. Non-tumor areas of the livers were also corrected for the same analyses. A pathologist with substantial experience in mouse liver histological analysis performed blind histological and immunohistochemical analysis.

- **QUANTIFICATION AND STATISTICAL ANALYSIS**

  Statistics and Reproducibility:

  We compared the 4 genotypes of mice given Alcohol-WD for tumor incidence. The *Tbc1d15$^{Flox/Flox}$:Ns5aTg* mice or *Numb-3A^{LSL}:Ns5aTg* mice *were* more likely to develop liver tumors compared to the *Alb-CreRT2;Tbc1d15$^{Flox/Flox}$:Ns5aTg* mice or *Numb-3A^{LSL}:Ns5aTg* mice *were* more likely to develop liver tumors compared or Alb::CreERT2*: Numb-3A^{LSL}:Ns5aTg* mice (using a 0.05-level chi-square test based on the 2x2 table using nQuery). We began with 25 mice in each group, ended up a minimum of 20 mice completed the experiments. Statistical analysis for biochemical/immunohistochemical parameters was performed as described above. A two-tailed t-test was used for most comparisons, with $p<0.05$ considered statistically significant. Data are presented as mean±S.D. Statistical analysis for biochemical parameters was performed as described above. For immunostaining of p-aPKCζ, p-NUMB, TBC1D15, p53, and NANOG, results

were reported as the percent of positive cells in each liver section. With 20 subjects in each of the four groups.

- **DATA AND SOFTWARE AVAILABILITY**
  - **NCBI tracking system number:**
    - The data used in this study has been deposited to NCBI under **GSE61435 (Microarray)** and **GSE68237 (ChIP-Seq)**.
    - Human Gene expression profiling by array[40]: **GSE17856** and **GSE27150**
    - The permanent URL to the Proteomics dataset is: ftp://massive.ucsd.edu/MSV000085321/

Supplementary Reference

1. Silvestri F*, et al.* The genotype of the hepatitis C virus in patients with HCV-related B cell non-Hodgkin's lymphoma. *Leukemia* **11**, 2157-2161 (1997).

2. Reya T, Morrison SJ, Clarke MF, Weissman IL. Stem cells, cancer, and cancer stem cells. *Nature* **414**, 105-111 (2001).

3. Clevers H. The cancer stem cell: premises, promises and challenges. *Nature medicine* **17**, 313-319 (2011).

4. Simonet WS, Bucay N, Lauer SJ, Taylor JM. A far-downstream hepatocyte-specific control region directs expression of the linked human apolipoprotein E and C-I genes in transgenic mice. *The Journal of biological chemistry* **268**, 8221-8229 (1993).

5. Majumder M*, et al.* Expression of hepatitis C virus non-structural 5A protein in the liver of transgenic mice. *FEBS letters* **555**, 528-532 (2003).

6. Machida K*, et al.* Toll-like receptor 4 mediates synergism between alcohol and HCV in hepatic oncogenesis involving stem cell marker Nanog. *Proceedings of the National Academy of Sciences of the United States of America* **106**, 1548-1553 (2009).

7. Chen CL*, et al.* NANOG Metabolically Reprograms Tumor-Initiating Stem-like Cells through Tumorigenic Changes in Oxidative Phosphorylation and Fatty Acid Metabolism. *Cell metabolism* **23**, 206-219 (2016).

8. Uthaya Kumar DB*, et al.* TLR4 Signaling via NANOG Cooperates With STAT3 to Activate Twist1 and Promote Formation of Tumor-Initiating Stem-Like Cells in Livers of Mice. *Gastroenterology* **150**, 707-719 (2016).

9. Feldman DE, Chen C, Punj V, Machida K. The TBC1D15 oncoprotein controls stem cell self-renewal through destabilization of the Numb-p53 complex. *PloS one* **8**, e57312 (2013).

10. Dapito DH*, et al.* Promotion of hepatocellular carcinoma by the intestinal microbiota and TLR4. *Cancer cell* **21**, 504-516 (2012).

11. Colaluca IN*, et al.* NUMB controls p53 tumour suppressor activity. *Nature* **451**, 76-80 (2008).

12. Siddique HR, Feldman DE, Chen CL, Punj V, Tokumitsu H, Machida K. NUMB phosphorylation destabilizes p53 and promotes self-renewal of tumor-initiating cells by a NANOG-dependent mechanism in liver cancer. *Hepatology* **62**, 1466-1479 (2015).

13. Onoue K*, et al.* Fis1 acts as a mitochondrial recruitment factor for TBC1D15 that is involved in regulation of mitochondrial morphology. *Journal of cell science* **126**, 176-185 (2013).

14. Wong YC, Ysselstein D, Krainc D. Mitochondria-lysosome contacts regulate mitochondrial fission via RAB7 GTP hydrolysis. *Nature* **554**, 382-386 (2018).

15. Peralta ER, Martin BC, Edinger AL. Differential effects of TBC1D15 and mammalian Vps39 on Rab7 activation state, lysosomal morphology, and growth factor dependence. *The Journal of biological chemistry* **285**, 16814-16821 (2010).

16. Zhang XM, Walsh B, Mitchell CA, Rowe T. TBC domain family, member 15 is a novel mammalian Rab GTPase-activating protein with substrate preference for Rab7. *Biochemical and biophysical research communications* **335**, 154-161 (2005).

17. Takahara Y*, et al.* Silencing of TBC1D15 promotes RhoA activation and membrane blebbing. *Molecular and cellular biochemistry* **389**, 9-16 (2014).

18. Berika M, Elgayyar ME, El-Hashash AH. Asymmetric cell division of stem cells in the lung and other systems. *Frontiers in cell and developmental biology* **2**, 33 (2014).

19. Williams SE, Beronja S, Pasolli HA, Fuchs E. Asymmetric cell divisions promote Notch-dependent epidermal differentiation. *Nature* **470**, 353-358 (2011).

20. Chang KC*, et al.* Ran GTPase-activating protein 1 is a therapeutic target in diffuse large B-cell lymphoma. *PloS one* **8**, e79863 (2013).

21. Speicher S, Fischer A, Knoblich J, Carmena A. The PDZ protein Canoe regulates the asymmetric division of Drosophila neuroblasts and muscle progenitors. *Current biology : CB* **18**, 831-837 (2008).

22. Gallini S*, et al.* NuMA Phosphorylation by Aurora-A Orchestrates Spindle Orientation. *Current biology : CB* **26**, 458-469 (2016).

23. Zhang Z*, et al.* Presenilins are required for gamma-secretase cleavage of beta-APP and transmembrane cleavage of Notch-1. *Nature cell biology* **2**, 463-465 (2000).

24. Dovey HF*, et al.* Functional gamma-secretase inhibitors reduce beta-amyloid peptide levels in brain. *Journal of neurochemistry* **76**, 173-181 (2001).

25. Feng J*, et al.* DAPT, a gamma-Secretase Inhibitor, Suppresses Tumorigenesis, and Progression of Growth Hormone-Producing Adenomas by Targeting Notch Signaling. *Frontiers in oncology* **9**, 809 (2019).

26. Lim CA*, et al.* Genome-wide mapping of RELA(p65) binding identifies E2F1 as a transcriptional activator recruited by NF-kappaB upon TLR4 activation. *Molecular cell* **27**, 622-635 (2007).

27. O'Neil J*, et al.* FBW7 mutations in leukemic cells mediate NOTCH pathway activation and resistance to gamma-secretase inhibitors. *The Journal of experimental medicine* **204**, 1813-1824 (2007).

28. Thompson BJ*, et al.* The SCFFBW7 ubiquitin ligase complex as a tumor suppressor in T cell leukemia. *The Journal of experimental medicine* **204**, 1825-1835 (2007).

29. Kovall RA, Blacklow SC. Mechanistic insights into Notch receptor signaling from structural and biochemical studies. *Current topics in developmental biology* **92**, 31-71 (2010).

30. McGill MA, McGlade CJ. Mammalian numb proteins promote Notch1 receptor ubiquitination and degradation of the Notch1 intracellular domain. *The Journal of biological chemistry* **278**, 23196-23203 (2003).

31. Noguchi M, Hirohashi S. Cell lines from non-neoplastic liver and hepatocellular carcinoma tissue from a single patient. *In vitro cellular & developmental biology Animal* **32**, 135-137 (1996).

32. Bogard AS, Tavalin SJ. Protein Kinase C (PKC)zeta Pseudosubstrate Inhibitor Peptide Promiscuously Binds PKC Family Isoforms and Disrupts Conventional PKC Targeting and Translocation. *Molecular pharmacology* **88**, 728-735 (2015).

33. Lim S*, et al.* A myristoylated pseudosubstrate peptide of PKC-zeta induces degranulation in HMC-1 cells independently of PKC-zeta activity. *Life sciences* **82**, 733-740 (2008).

34. Lee SR, Sang L, Yue DT. Uncovering Aberrant Mutant PKA Function with Flow Cytometric FRET. *Cell reports* **14**, 3019-3029 (2016).

35. Banning C*, et al.* A flow cytometry-based FRET assay to identify and analyse protein-protein interactions in living cells. *PloS one* **5**, e9344 (2010).

36. Zhou Y*, et al.* Rapid and enhanced proteolytic digestion using electric-field-oriented enzyme reactor. *Journal of proteomics* **74**, 1030-1035 (2011).

37. Machida K, Liu JC, McNamara G, Levine A, Duan L, Lai MM. Hepatitis C virus causes uncoupling of mitotic checkpoint and chromosomal polyploidy through the Rb pathway. *Journal of virology* **83**, 12590-12600 (2009).

38. Feldman DE, Chen C, Punj V, Tsukamoto H, Machida K. Pluripotency factor-mediated expression of the leptin receptor (OB-R) links obesity to oncogenesis through tumor-initiating stem cells. *Proceedings of the National Academy of Sciences of the United States of America* **109**, 829-834 (2012).

39. Raafat A*, et al.* Expression of Notch receptors, ligands, and target genes during development of the mouse mammary gland. *Journal of cellular physiology* **226**, 1940-1952 (2011).

40. Tsuchiya M, Parker JS, Kono H, Matsuda M, Fujii H, Rusyn I. Gene expression in nontumoral liver tissue and recurrence-free survival in hepatitis C virus-positive hepatocellular carcinoma. *Molecular cancer* **9**, 74 (2010).

41. Gavaler JS. Effects of alcohol on endocrine function in postmenopausal women: a review. *Journal of studies on alcohol* **46**, 495-516 (1985).

42. Kim DK*, et al.* Estrogen-related receptor gamma controls hepatic CB1 receptor-mediated CYP2E1 expression and oxidative liver injury by alcohol. *Gut* **62**, 1044-1054 (2013).

43. Zhou F, Sikorski TW, Ficarro SB, Webber JT, Marto JA. Online nanoflow reversed phase-strong anion exchange-reversed phase liquid chromatography-tandem mass spectrometry platform for efficient and in-depth proteome sequence analysis of complex organisms. *Analytical chemistry* **83**, 6996-7005 (2011).

44. Laudanna C*, et al.* Motility analysis of pancreatic adenocarcinoma cells reveals a role for the atypical zeta isoform of protein kinase C in cancer cell movement. *Laboratory investigation; a journal of technical methods and pathology* **83**, 1155-1163 (2003).